AFFDL-TR-66-14

STIFFNESS AND VIBRATION CHARACTERISTICS OF INFLATABLE DELTA WING MODELS AT TEMPERATURES UP TO 650°F

SAMUEL J. POLLOCK

FOREWORD

This report was prepared by the Aerospace Dynamics Branch, Vehicle Dynamics Division, Air Force Flight Dynamics Laboratory, Wright-Patterson Air Force Base, Ohio. The work was performed to provide information on dynamic thermoelastic properties of inflatable structures for re-entry vehicle applications considered by the Space Systems Division. It is part of the Research and Technology Division, Air Force Systems Command's exploratory development program. This research was conducted under Project No. 1370, "Dynamic Problems in Flight Vehicles," and Task No. 137003, "Prediction and Prevention of Dynamic Aerothermoelastic Instabilities." Mr. S. J. Pollock was the project engineer. This report covers research conducted from October 1963 to October 1965.

The tests were conducted in the AFFDL Structural Test Facility, WPAFB, Ohio, under the direction of Mr. J. B. Monfort of the AFFDL Structures Division. Instrumentation and data reduction were performed by Mr. J. R. Pokorski of the Structures Division for the static tests and by Messrs. E. R. Hotz and L. P. Vaughn of the Vehicle Dynamics Division for the vibration tests. Mr. J. P. Hudson of the Digital Computation Division provided the computer solutions for the program. Inflatable Airmat models were fabricated by Goodyear Aerospace Corporation under Contract AF33(615)-1880 with Mr. R. W. Nordlie as GAC project engineer. Technical comments were obtained from Professor J. W. Mar and Mr. J. R. Martuccelli of the Massachusetts Institute of Technology and are gratefully acknowledged.

Manuscript released by the author 29 October 1965 for publication as an AFFDL Technical Report.

This report has been reviewed and is approved.

Walter J. Mykytow
WALTER J. MYKYTOW
Asst. for Research & Technology
Vehicle Dynamics Division

ABSTRACT

Stiffness and vibration data were obtained on inflatable Airmat* models for various internal pressures from two to ten psi and temperatures up to 650°F. The semi-span 65 degree delta wing models were woven from stainless steel monofilament wire and coated with high temperature silicone elastomer. Deflection and vibration characteristics were predicted using shear theory. Vibration predictions were also made using measured influence coefficients.

Shear theory was found to be in good agreement with experiment for deflections due to uniform load except near the leading edge where experimental deflections were smaller than predicted due to the stiffening effect of the rounded edges. Correlation of shear theory prediction for vibration frequencies with experiment improved as internal pressure increased to 10 psi. Vibration calculations using measured small deflection influence coefficients were in good agreement with experiment.

Temperature effects on model vibration characteristics were determined. Model frequencies decreased as temperature was increased from 70°F to about 300°F. For temperatures from 300°F to 650°F, vibration frequencies increased. At 650°F the vibration frequency for a model without ceramic frits in the silicone elastomer coating was as much as 32 percent higher than the room temperature frequency. For a model with ceramic frits in the silicone elastomer coating the frequency at 650°F was as much as 10 percent lower than the room temperature frequency. Mode shapes did not change appreciably with temperature. Structural damping coefficients decreased with increasing temperature.

*Trademark of Goodyear Aerospace Corporation

TABLE OF CONTENTS

LIST OF ILLUSTRATIONS

LIST OF TABLES

SYMBOLS

C	Flexibility influence coefficient, in/lb.
c	Root chord, inches
f	Load intensity, psi
g	Structural damping coefficient
h	Model thickness, inches
m	Mass, lb sec^2/in
p	Pressure differential, psi
q	Total load, lbs; also generalized coordinate in Section V
t	Airmat cover skin thickness, also time
w	Vertical deflection, inches (positive down)
x,y	Cartesian coordinates, See Figure 1
α	Angle of drop cord rotation in x-direction, See Section V
β	Angle of drop cord rotation in y-direction, See Section V
λ	Eigenvalue, See Section V
μ	Poisson's ratio, See Section V
ω	Frequency, radians per second

SECTION I

INTRODUCTION

The use of inflatable structures for winged entry vehicles is attractive because of the good packaging characteristics during boost and reduced aerodynamic heating provided by low wing loading during re-entry. The highly flexible nature of inflatable materials means that their structural dynamic properties must be given special consideration. Thermoelastic properties of inflatables are required to evaluate dynamic characteristics at hypersonic speeds.

A process of weaving metal fabric structures, developed by Goodyear Aerospace Corporation, has the trade name "Airmat". Several investigators have studied the stiffness and vibration characteristics of inflatable structures constructed of nylon, dacron, or metal fabric. Analytical and experimental investigations of inflatable fabric platelike structures were performed by Leonard, et al (Reference 8), McComb (Reference 9) and Stroud (Reference 10). Influence coefficients have been determined for inflatable delta wing models and used to predict vibration characteristics by Seath (Reference 7), Martuccelli, et al (References 2, 4 and 5) and Mar (Reference 3). Aeroelastic characteristics of inflatable Airmat delta wing models have been determined for subsonic through hypersonic speeds by the Aeroelastic and Structures Research Laboratory of the Massachusetts Institute of Technology (References 4 and 5). All of the previous investigations, except those by MIT, were for inflatable structures at room temperature. The prediction and evaluation of dynamic characteristics of inflatables at hypersonic speeds requires a knowledge of the effect of temperature on stiffness characteristics. Since material properties of this relatively new construction have not been established, this effect must be determined through tests. This program extends results obtained by MIT on smaller models to higher temperatures. Also, more detailed vibration data, more extensive influence coefficient data, and deflections due to a uniform load were obtained.

The purpose of this investigation was to determine the static and vibration characteristics of inflatable Airmat models at temperatures up to 650°F for various model internal pressures. The 65 degree sweep delta wing models with a root chord length of 51.1 inches chosen for this investigation are geometrically similar to the flutter models of Reference 5, which had a root chord length of 24 inches. Stiffness and vibration properties of three inflatable delta wing models were determined by uniform load, influence coefficient, and vibration tests at temperatures up to 650°F. Deflection and vibration predictions using available theories and measured influence coefficients are correlated with experimental results.

SECTION II

MODEL DESCRIPTION

The Airmat models investigated had a nominal leading edge sweep angle of 65 degrees. The root chord was 51.1 inches and the trailing edge span was 24.5 inches. The models were 3 inches thick and had rounded leading and trailing edges. Figure 1 is a sketch of the model and base plate showing the coordinate system used in the report.

The model structure consists of two basic materials; woven stainless steel Airmat, and a silicone elastomer coating. The Airmat material is the basic wing structure when inflated and the elastomer coating makes internal pressurization possible.

The Airmat material was woven from Type 304 annealed stainless steel wire .0045 inches in diameter. The Airmat faces have 98 wires per inch in both the warp and fill direction. The drop wires are of the same material and there are 31.2 drop wires per square inch. The warp direction of the Airmat is oriented parallel to the base plate.

Models one and two were coated with S-2077 silicone elastomer while model three was coated with CS-105 silicone-ceramic elastomer. Dow Corning Corporation's S-2077 silicone elastomer is a proprietary composition of a silicone polymer, filler, binder, plasticizer, and vulcanizing agent. The CS-105 elastomer consists of S-2077 loaded with Harshaw Chemical's AW-35 ceramic frit. Reference 6 contains an evaluation of the coatings. The white S-2077 coating is considered adequate for temperatures up to 800°F while the black CS-105 coating is used for higher temperature applications.

The first step in the model fabrication is cutout of the Airmat material. The drop wires in the leading and trailing edges are then clipped back to allow the top and bottom faces to be brought together, lapped, and resistance spot welded. This provides semi-cylindrical leading and trailing edges when the models are inflated. The drop wires in the base plate area are then clipped back to the inside of the plate and the base plate inserted. Airmat attachment to the base plate is by resistance spot welding. A clamping bar is provided around the periphery of the base plate after the Airmat has been attached and coated. This clamping bar prevents tension loading on the spot welds that attach the Airmat to the base plate. The clamping bar is Type 410, Condition A, stainless steel 5/16 inch thick and 15/16 inch wide. The clamping bar is attached to the base plate by No. 8 stainless steel screws with approximately two inch spacing.

A number of stainless steel discs are welded to the upper and lower surfaces of the Airmat models prior to coating. The location of these discs is given in Table 1. The discs on the upper surface are 1/4 inch in diameter and approximately 1/8 inch thick. The discs on the lower surface are 1/2 inch in diameter and approximately 1/16 inch thick. The Airmat assembly is next cleaned and coated with elastomer. After the coating is cured the clamping bars are fitted and attached. Further information on model properties and construction is contained in References 14 and 15.

The actual weights of the three models, not including the base plate, were:

Model One - 2.83 lbs.

Model Two - 2.86 lbs.

Model Three - 3.65 lbs.

Figures 2 and 3 are two views of model one in the test jig. The base plate for attaching the models to the test jig is of type 410 stainless steel bar stock one-half inch thick. The material was heat treated to a minimum of 125,000 psi tensile ultimate strength. Sixteen, three-eighths inch diameter, tapped holes are provided for attachment to the test jig. Pipe threaded holes are also provided in the base plate for attachment of air inlet and pressure gage fittings. The pressurization system is shown schematically in Figure 4. Figure 5 is a view of the pressurization equipment showing the manometer used to monitor pressure in the models during tests.

SECTION III

INSTRUMENTATION

A. DEFLECTION TRANSDUCERS

Standard deflection potentiometers were modified by removing the spring and adding a pulley and weight system to reduce the load on the model. The wires from the transducers were attached to the lower surface of the models by hooks welded to the 1/2 inch discs discussed in the previous section. Figure 6 shows ten transducers attached to model two for measuring static deflections. Twelve deflection transducers were used for model one, and ten transducers for models two and three. Figure 7 is a view of the lower surface of model one showing twelve hooks.

B. THERMOCOUPLES

Thermocouples were installed on the models by Goodyear Aerospace Corporation for use in controlling and monitoring the model skin temperature. Additional thermocouples were installed by the Air Force Flight Dynamics Laboratory personnel to obtain better temperature control. The thermocouples are Chromel-Alumel (ISAK) type.

C. ACCELEROMETERS

Endevco Model 2226 accelerometers were attached at six of the loading points on the upper surface of model one by Eastman 910 glue. These accelerometers weigh only 0.1 ounce each and should not significantly affect the model vibration characteristics. Figure 8 shows this accelerometer installation for room temperature vibration tests on model one.

Modified accelerometer mounting studs were made interchangeable with the deflection transducer hooks on the lower surfaces of models two and three. Ten Endevco Model 2245B accelerometers were attached to the lower surface of model two for the room and elevated temperature vibration tests as shown in Figure 9. These accelerometers are capable of operation at temperatures up to 750°F and weigh about one ounce each. Since there are ten of these accelerometers on the model and the model weighs less than three pounds, the accelerometers have a significant effect on vibration characteristics. For the inflatable model considered as a simple spring-mass system, the resonant frequency is reduced by about ten percent due to the added mass of the ten accelerometers. Since only qualitative information on mode shapes and frequencies were required, no corrections were made to the measured vibration data. In order to obtain vibration data on model three at temperatures above 750°F, an accelerometer was attached at the bottom of the shaker where it was shielded from the high temperatures.

D. PRESSURE TRANSDUCER

Pressure was recorded by a Data Sensors, Inc. model PB536G-1 pressure transducer with a range of 0 - 15 psig. The transducer inaccuracy is ± .0465 psig.

SECTION IV

TEST PROCEDURES

A. UNIFORM LOAD

Uniform load tests were conducted on models one and two (silicone elastomer coating without ceramic frits) at room temperature with internal pressures of 2, 4, 6, 8, and 10 psi. The uniform loading was accomplished by means of small bags containing lead shot placed over the planform of the wing. The deflections were simultaneously recorded for all of the transducers. Figures 10 and 11 show model one at an internal pressure of 2 psi with a total load of 20 pounds uniformly distributed over the model.

B. INFLUENCE COEFFICIENTS

Influence coefficients were obtained for model one at internal pressures of 2, 4, 6, 8, and 10 psi at room temperature and 2, 6, and 10 psi at 650°F. Twelve load points for influence coefficient tests are located on the top surface of model one as shown in Figure 2. Figure 6 shows the method of loading. Loading plates with diameters of 2.75 inches were placed on the loading points in order to avoid excessive local deformations. The loading plates contained a depression to allow accurate positioning of the loading rod.

Deflection readings were taken at all 12 points on the model for zero load and three other loads applied at each point. Only deflections measured for increasing load increments were used to determine influence coefficients. From these data the deflection versus load was plotted. A typical plot is shown in Figure 12. This procedure was repeated until loads had been applied at all 12 points. A total of 1152 plots were required to establish 12 x 12 flexibility influence coefficient matrices for five different pressures at room temperature and three different pressures at 650°F. As shown in Figure 12, the deflection versus load relationship was not linear. Also, deflections measured during unloading were significantly different from those obtained during load application, indicating the presence of large hysteresis effects. The same behavior was reported for the delta wing models of Reference 5.

C. VIBRATION TESTS

Vibration tests were conducted on all three of the inflatable models. A five pound force electro-magnetic shaker was attached near the tip of the models as shown in Figures 8 and 9. A long rod was attached to the shaker and to the model. The fundamental frequency of the rod was not within the range of excitation frequencies used during the vibration tests. The output from the accelerometers was observed on a voltmeter or an oscilloscope and the frequency obtained from an electronic counter. The data were recorded on a tape recorder and/or on an oscillograph for analysis. Some of the vibration test equipment used for model one is shown in Figure 13 and some of the equipment used for model two is shown in Figure 14. Vibration tests were conducted at room temperature on all of the models. In addition, model two was tested at 500°F and 650°F. Model three (silicone elastomer coating with ceramic frits) was also tested at 300°F, 500°F, 650°F, and 800°F.

Damping was determined by shutting off the excitation of the model at the shaker. The damping coefficient was determined from the logarithm of the ratio between the amplitudes of successive cycles in the decay curve.

Node lines were obtained at room temperature by sprinkling white sand, coffee grounds, or sunflower seeds over the surface of the model and observing the nodal pattern for the various modes. At elevated temperatures, mode shapes were obtained from the accelerometer data.

SECTION V

SHEAR THEORY

A. STRAIN-ENERGY APPROACH

A simplified method of computing deflection and frequency characteristics of inflatable plates is derived in Reference 4. This section contains a summary of the method and results of its application to the delta wing models. The strain energy expression for an inflatable Airmat plate of uniform thickness, h, undergoing small deformations is

$$U_s = \frac{h^2}{4} \iint_s \left\{ A_{11}\, \alpha_x^2 + A_{22}\, \beta_y^2 + (A_{12} + A_{21})\, \alpha_x\, \beta_y + A_{33}\, (\alpha_y + \beta_x)^2 \right\}$$

$$dx\, dy + 1/2 \iint_s ph \left\{ (\alpha + w_x)^2 + (\beta + w_y)^2 \right\} dx\, dy$$

where the pressure, p, has been substituted for the shear modulus, G, in the stress-strain relations. The drop chords remain straight and rotate to an angle α from the vertical in the x-direction and β from the vertical in the y-direction. Subscripts x and y represent differentiation with respect to x and y, respectively. If the surfaces are treated as orthotropic with the x- and y- axes aligned with the principal directions then

$$A_{11} = \frac{E_1\, t}{1-\mu_{12}\, \mu_{21}} \qquad A_{12} = A_{21} = \frac{\mu_{21}\, E_1 t}{1 - \mu_{12}\mu_{21}}$$

$$A_{22} = \frac{E_2\, t}{1-\mu_{12}\, \mu_{21}} \qquad A_{33} = Gt$$

$E_1\, t$, and $E_2 t$ are the extensional stiffnesses in the x- and y- directions, respectively. μ_{12} (or μ_{21}) is the Poisson's ratio associated with a contraction in the y- (or x-) direction caused by a tensile stress in the x- (or y-) direction.

If the bending deflections are considered negligible in comparison with shear deflections, that is, deformations are purely of the shear type then $\alpha = \beta = 0$ and the strain energy becomes

$$U_s = \frac{1}{2}\iint_s ph\,(w_x^2 + w_y^2)\,dx\,dy$$

Using the Rayleigh-Ritz method, the deflection, w, is represented by

$$w\,(x,y,t) = \sum_{n=1}^{N} q_n\,(t)\,w_n\,(x,y)$$

where the quantities $q_n(t)$ are generalized coordinates and $w_n\,(x,y)$ are assumed displacement functions that satisfy the geometric boundary conditions. The following powers of $\bar{x}$ and $\bar{y}$ are chosen

$w_1 = \bar{y}$ $\quad w_2 = \bar{x}\bar{y}$ $\quad w_3 = \bar{y}^2$ $\quad w_4 = \bar{x}^2\bar{y}$

$w_5 = \bar{x}\bar{y}^2$ $\quad w_6 = \bar{y}^3$ $\quad w_7 = \bar{x}^2\bar{y}^2$ $\quad w_8 = \bar{x}\bar{y}^3$

and $w_9 = \bar{y}^4$ where $\bar{x} = {}^x/_c$ and $\bar{y} = {}^y/_c$

B. VIBRATION PREDICTION

The kinetic energy is formed and the homogeneous form of Lagrange's equation is applied to give an eigenvalue problem. The eigenvalue is given by

$$\lambda = \frac{\omega^2\,\bar{m}\,c^2}{ph}$$ where $\bar{m}$ is the mass per unit area.

For a 65 degree delta the first three eigenvalues are found in Reference 4 to be:

$\lambda_1 = 19.224$, $\lambda_2 = 77.549$, $\lambda_3 = 147.32$ with the associated eigenvectors:

$$q^{(1)} = \begin{Bmatrix} -0.011 \\ 0.106 \\ -0.198 \\ 0.053 \\ 1.000 \\ -0.873 \\ -0.906 \\ 0.772 \\ 0.031 \end{Bmatrix} \qquad q^{(2)} = \begin{Bmatrix} 0.035 \\ -0.313 \\ -0.167 \\ 0.304 \\ 1.000 \\ -0.253 \\ -0.964 \\ 0.746 \\ -0.567 \end{Bmatrix} \qquad q^{(3)} = \begin{Bmatrix} -0.037 \\ -0.533 \\ 0.642 \\ 0.962 \\ 1.000 \\ -2.943 \\ -2.714 \\ 0.808 \\ 4.851 \end{Bmatrix}$$

The vibration frequencies from the predicted eigenvalues are presented in Tables 3, 4, and 5 for the first three modes of models one, two, and three, respectively. The node lines calculated from the eigenvectors are shown in Figure 22 for the second and third modes.

C. DEFLECTION PREDICTION

The deflection under a uniform static load can be calculated from the solution to the non-homogeneous Lagrange's equation given in Reference 4. For a 65 degree delta wing this equation reduces to the following:

$$w\ (x,y) = \frac{c^2\ f}{ph} \left\{ 0.3698\ \bar{y} - 0.0622\ \bar{x}\bar{y} - 0.5338\ \bar{y}^2 - 0.3139\ \bar{x}^2\bar{y} + 0.2795\ \bar{x}\ \bar{y}^2 + 0.2084\ \bar{y}^3 - 0.3383\ \bar{x}^2\bar{y}^2 - 0.3426\ \bar{x}\bar{y}^3 - 0.0173\ \bar{y}^4 \right\}$$

where f is the load intensity in psi and

$\bar{x} = x/_c$, $\bar{y} = y/_c$.

Predicted deflections are presented in Table 6 and compared with experiment for models one and two at an internal pressure of 2 psi in Figure 15.

SECTION VI

RESULTS

A. STATIC TESTS AND CORRELATION

1. UNIFORM LOAD

Uniformly distributed static loads were applied at room temperature to models one and two, which do not have ceramic frits in the coating. Model internal pressures were 2, 4, 6, 8, and 10 psi. The resulting static vertical deflections are presented in Tables 7 and 8 for models one and two, respectively. The results were essentially the same for both models at the same loading and pressure conditions.

Figure 15 presents vertical deflections from the uniform load tests, together with shear theory predictions for an internal pressure of 2 psi. The only significant differences occur for points 36 and 36N which are located near the leading edge of models one and two, respectively. The experimental deflections for these points are always lower than predicted. This is caused by the stiffening effect of the rounded edges which is not accounted for by the theory. It should also be noted that the predicted deflection at point 36N is higher than that at 36, since 36N is one inch farther from the root than 36. However, the experimental deflections are always less for point 36N than for point 36. This is a further demonstration of the stiffening effect of the rounded leading edge. Good agreement was obtained between experiment and shear theory predictions for points away from the edges of the models.

2. INFLUENCE COEFFICIENTS

The flexibility influence coefficients obtained from the measured deflection-load data are presented in the Appendix. The technique for obtaining the influence coefficients from the data is illustrated in Figure 12. Two sets of influence coefficients were calculated. The first set of influence coefficients represented a straight-line approximation to the measured data, omitting the zero load point. When used in vibration analyses these influence coefficients predicted first mode vibration frequencies which were as much as 12 percent lower than experiment. This indicated that the calculated flexibility influence coefficients were too large, causing the predicted stiffness to be lower than the actual model stiffness. Therefore, the influence coefficients were recalculated by drawing a curve through the measured deflection-load points and using a tangent to the curve at the zero load point. Since the model was vibrated at small amplitudes, these tangent-curve influence coefficients yielded more accurate vibration predictions.

By Maxwell's law of reciprocal deflections for an elastic structure, $C_{ij} = C_{ji}$ where C_{ij} is the influence coefficient for the deflection at i due to a load at j and C_{ji} is the influence coefficient for the deflection at j due to a load at i (Reference 13). The experimental values for C_{ij} and C_{ji} differed considerably in some instances. Since the structure did not obey Maxwell's law, the inflated wing is not behaving elastically. Similar behavior was reported in Reference 3 for the inflatable delta wing models of that study. The largest discrepancies were for stations near the root on the forward part of the model. Some of the influence coefficient matrices were made symmetrical by averaging the C_{ij} and C_{ji} terms. When these symmetrical influence coefficients were used in vibration calculations, no appreciable difference was noted in the predicted vibration frequencies or in the eigenvectors as compared to calculations using the unsymmetrical measured coefficients.

B. VIBRATION TESTS AND CORRELATION

1. EXPERIMENT

Measured vibration frequencies, structural damping coefficients and mode shapes are contained in Tables 9 through 16.

a. Temperature Effects

The measured room temperature vibration characteristics for model one (no ceramic frits in coating) are presented in Table 9. Table 10 gives the same characteristics after the model was held at 650°F for approximately five hours to obtain influence coefficient data, then cooled to room temperature. When the models are exposed to temperatures of 650°F or higher crazing occurs after cooling. The coating becomes flaky and tends to crack if flexed. The first mode frequency was about 16 percent higher for an internal pressure of 2 psi after the 650°F test. However, at internal pressures of 4, 6, 8, and 10 psi the first mode frequencies after the 650°F test were essentially the same as before the test. The relative amplitude in the first mode was the same except near the leading edge where it was reduced to about 1/4 the value prior to the 650°F test for all model internal pressures. There was practically no change in the second and third mode frequencies or mode shapes.

Figure 16 shows the effect of temperature on the first vibration mode frequency of models two and three at 10 psi (model two was coated with S-2077 elastomer without ceramic frits and model three was coated with the CS-105 elastomer which contains ceramic frits). Data were obtained at about 70°F, 300°F, 500°F, and 650°F. Vibration frequencies decreased from about 70°F up to about 300°F and then increased from about 300°F to 650°F. The vibration frequency varies most rapidly at room temperature. The first mode frequency of model three at an internal pressure of 2 psi changed by six percent as the room temperature changed from 68°F to 73°F. The trends with temperature were generally found to be similar to those observed in Reference 5. In Reference 5 it was determined by tests at small increments of temperature that the minimum frequency occurred at about 300°F. The curves of Figure 16 were drawn to incorporate these previously observed trends. At 650°F the first vibration mode frequency for model two was as much as 32 percent higher than at room temperature while the frequency for model three was about ten percent lower than at room temperature. The mode shapes for model two at 500°F and 650°F do not change appreciably from room temperature values as can be seen from the limited amount of data presented in Table 13.

b. Structural Damping

The structural damping coefficients for model two are presented in Table 11. In the first mode the damping coefficient at room temperature was about 0.15. This is higher than most conventional structures. In higher modes the damping coefficient decreased to as low as 0.02 for the fifth mode. At 650°F the damping coefficient decreased to as low as 0.04 in the first mode and .008 in the fifth mode. The damping coefficient, g, depends on the amplitude of vibration and is higher for higher amplitudes.

c. Effect of Shaker Weight

Since the models weigh less than four pounds and the effective weight of the vibration equipment attached to the models was about 0.6 pounds, tests were conducted to determine the effect of this additional mass on the natural vibration frequencies. Figure 17 shows the effect on the first two vibration mode frequencies of model three for three different pressures due to weight added to the shaker at the point of attachment to the model. If a curve is drawn through the experimental points and extrapolated to zero the first mode test frequency is lowered by an average of nine percent and the second mode test frequency is lowered by an average of seven percent from the system with no added weight. The decrease in frequency due to the added mass calculated for a simple spring-mass system is slightly over eight percent. The vibration data in this report are presented with no corrections for the added mass of the shaker attached to the tip of the models during vibration tests. However, this could be accounted for if desired.

d. Effect of Vibration Amplitude

The vibration frequency was found to depend nonlinearly on amplitude of vibration, being higher at lower amplitudes. The amplitude of excitation was kept small during the tests in order to minimize variations in the frequency due to amplitude. This nonlinear behavior was also reported for the flutter models in Reference 5.

e. Mode Shapes

Figure 18 presents a comparison of node lines observed for models one and two (no ceramic frits in coating) with node lines presented in Reference 5 for inflatable flutter models. Both the models of this study and the Reference 5 flutter models are geometrically similar. However, the flutter models contained 49 drop wires per square inch, were coated with the CS-105 elastomer containing ceramic frits, and were excited acoustically using a speaker while models one and two contained 31.2 drop wires per square inch, were coated with the S-2077 elastomer without ceramic frits, and were excited using a shaker attached to the model. Since the models were all cantilevered for vibration tests the node line for the first mode is along the root and is not shown in Figure 18. Node lines for models one and two are somewhat similar to those of the Reference 5 flutter models except for the fourth mode.

The measured mode shapes for models one and two were normalized and the results are presented in Tables 9, 10, and 12. The relative amplitude in the first mode for model two at point 36N is less than that at point 35 at all internal pressures although 36N is five inches farther from the root than 35. This is due to the leading edge stiffness effects previously discussed.

f. Model Three Failure

Model three (ceramic frits in coating) burst during hot vibration tests. The conditions at failure were an internal pressure of 10 psi and a uniform temperature of approximately 800°F. The temperature distribution prior to failure is given in Reference 11. Smoke was observed before the explosion and the drop cords appeared to have failed in tension. This type failure was unexpected since the calculated internal pressure for average ultimate strength of the stainless steel drop wires was about 32 psi at 800°F. Two views of the failed model are shown in Figures 19 and 20.

2. VIBRATION PREDICTION USING SHEAR THEORY

Figure 21 presents a comparison between shear theory predictions and experiment for the first vibration mode frequency versus pressure for model three (ceramic frits in coating). These results are for room temperature conditions. The vibration frequency predicted by shear theory is 40 percent lower than experiment at a model internal pressure of 2 psi. As internal pressure is increased, agreement between shear theory and experiment improves and the predicted value for the first mode frequency is 20 percent lower than experiment at 6 psi and 9 percent lower than experiment at 10 psi. For pressures investigated in Reference 5 (up to 6 psi), similar results were obtained. Agreement between shear theory predictions and experiment was better for the first vibration mode frequency of model one which had no ceramic frits in the coating; the predicted frequency was only 17 percent lower than experiment at 2 psi and two percent lower at 10 psi. Similar results were obtained for correlation of predicted second and third vibration mode frequencies with experiment.

In Figure 22 the node lines predicted from the vibration analysis using shear theory are compared with the experimental node lines for the second and third modes of models one and two (no ceramic frits in coating). The predicted node line for the second mode is in good agreement with experiment, but the predicted node line for the third mode deviates somewhat from experiment.

The vibration frequencies plotted versus pressure on a log-log scale in Figures 23 and 24 are straight lines. This indicates that the frequency is an exponential function of the model internal pressure. The exponent is about 1/4 for the first mode and approaches 1/2 for the higher modes. Shear theory predicts an exponent of 1/2.

3. VIBRATION PREDICTION USING INFLUENCE COEFFICIENTS

The calculated vibration frequencies and eigenvectors using flexibility influence coefficients, which were measured only for model one (coating without ceramic frits), are presented in the Appendix in Tables 34 through 53. A brief description of the vibration analysis method is also presented in the Appendix. The predicted room temperature vibration frequencies are compared with experimental frequencies in Figure 23. Vibration predictions were made using influence coefficients based on both tangent-curve approximation at the zero load point and straight-line approximation omitting the zero load point as described previously in part A2 of this section. Calculated vibration frequencies for the first two modes using influence coefficients based on tangent-curve approximations were about five percent higher than the corresponding calculations for straight-line approximations. This five percent increase in frequency greatly improved the correlation between calculated and experimental frequencies. The predicted first and second vibration mode frequencies using tangent-curve influence coefficients are below experiment by 6.0 and 4.5 percent, respectively. This is believed to be within the accuracy of the experimental techniques. Some uncertainties in the measured influence coefficients used in vibration predictions were caused by nonlinear load-deflection characteristics, large hysteresis effects, and inelastic behavior of the structure. Measured vibration frequency uncertainties result from nonlinear dependence on amplitude of excitation and extreme sensitivity to variations in temperature around 70°F.

The first mode vibration frequencies calculated with the shaker rod mass included in the mass matrix averaged 17 percent lower than the corresponding values without the shaker rod mass included. Higher mode frequencies were reduced by a smaller percentage. Experimental results indicated that the shaker mass lowered the first mode frequency by about nine percent. Vibration predictions using the model mass matrix, not including the shaker rod mass, are used in the correlations with experiment.

Figure 24 gives the first three vibration mode frequencies calculated for model one based on influence coefficients measured at 650°F. The predicted first mode frequency at 2 psi and 650°F is about 11 percent higher than the predicted room temperature value. At 10 psi and 650°F the predicted first mode frequency is about 1.5 percent higher than the predicted room temperature value. This predicted rise in frequency from room temperature to 650°F was observed during vibration tests of model two which has the same type of coating as model one. For model two the increase in the first vibration mode frequency at 650°F was 32 percent at 2 psi and 9 percent at 10 psi. The predicted and observed increase in second and higher vibration mode frequencies at 650°F was less than for the first mode. The predicted vibration mode shapes are contained in Tables 42 through 53. A comparison of Tables 42 and 48 indicates that the mode shapes predicted for the first mode of model one at 650°F are not significantly different from the room temperature mode shapes. However, from Tables 43 through 47 and 49 through 53, the second and higher vibration mode shapes at 650°F are altered considerably from the comparable values at room temperatures.

In Figure 25, node lines interpolated from vibration calculations using influence coefficients measured at room temperature are compared with the corresponding experimental node lines. Agreement between predictions and experiment is reasonable for the first five modes except for the fourth mode. The node lines for the fourth mode predicted by calculations based on influence coefficients are similar to the experimental node lines observed for the fourth mode of the models of Reference 5.

SECTION VII

CONCLUSIONS

From this analytical and experimental investigation of inflatable Airmat delta wing structures, it is concluded that:

1. Vibration calculations using influence coefficients, based on drawing a tangent to the measured deflection-load curve at the zero load point, gave satisfactory correlation with experiment. The tangent-curve approximation was required because of the nonlinear deflection-load behavior and the small vibration amplitudes. Locating some of the stations for influence coefficients closer to the leading and trailing edges of the models would probably improve correlation of vibration predictions with experiment since these rounded edges act as stiffeners or spar-beams.

2. Shear theory predictions for the first vibration mode frequencies were lower than experiment by as much as 40 percent at 2 psi, but only 9 percent at 10 psi. This indicates that shear theory provides a relatively good structural representation for higher internal pressures; but for low internal pressures, metal fabric bending terms must also be included in the analysis for good vibration prediction.

3. For deflections due to a uniformly distributed load good agreement was obtained between shear theory predictions and experiment. Some local discrepancies occurred close to the leading edge where the experimental deflections were smaller than predicted. This again demonstrates the stiffening effect of the rounded leading edges, which is not accounted for in the theory.

4. When inflatable structures with silicone elastomer coatings are exposed to temperatures above 500°F, and then cooled to room temperature, the coating becomes flaky and tends to crack if flexed. After cooling to room temperature, the first vibration mode frequency is considerably altered while higher mode frequencies are relatively unaffected. For a model without ceramic frits in the silicone elastomer coating the first vibration mode frequency was about 16 percent higher at 2 psi after the model was heated to 650°F and then cooled.

5. The effects of high temperature on vibration were somewhat different for the two types of coating. For the model with the CS-105 elastomer coating (with ceramic frits), the first mode frequency at 650°F was about 10 percent below the room temperature value, whereas for the model coated with the S-2077 elastomer the frequency was as much as 32 percent above the room temperature value. Similar results were obtained for the second and higher vibration mode frequencies although the percentages were less.

6. Additional analytical and experimental work on inflatable structures is needed in the following areas to improve accuracy of prediction methods and increase confidence in the design of inflatable structures for re-entry applications:

a. The free edges of the delta wing models with rounded leading and trailing edges act as stiffeners or spar-beams. These edges should be included in the structural analysis as discrete elements to attempt to improve agreement between theory and experiment.

b. A better knowledge of the stiffness properties of the surface material is required so that bending-type deformations can be included in structural dynamic analyses for low internal pressures where these bending terms may become important. Bending terms were not included in the analyses of this report.

c. The determination of scaling laws for inflatable structures is required so that these results can be used in preliminary design of full-scale inflatable wings.

SECTION VIII

REFERENCES

1. P. N. Gustafson and R. J. Duffin; Natural Vibrations of Cantilevered Triangular Plates, II, WADC TR 54-358, July 1954.

2. J. R. Martuccelli, F. H. Durgin, and R. B. McCallum, "Construction and Testing Techniques of Inflatable Flutter Models", RTD-TDR-63-4197, Part I, Proceedings of Symposium on Aeroelastic and Dynamic Modeling Technology, March 1964.

3. J. W..Mar, Static and Vibration Behavior of Inflated Rectangular and Delta Planform Plates, AFFDL-TR-65-203, January 1966.

4. J. R. Martuccelli, G. Zartarian and R. B. McCallum, Aeroelastic Investigations of Inflatable Lifting Surfaces, FDL-TDR-64-147, February 1965, Confidential Report.

5. J. R. Martuccelli, G. Zartarian and R. B. McCallum, Dynamic Aerothermoelastic Instabilities of Inflatable Vehicles at Hypersonic Speeds, AFFDL-TR-65-177, December 1965, Confidential Report.

6. W. B. Cross, D. M. Marco, and F. Nass, New and Improved Materials for Expandable Structures (Phase III - Re-entry Coatings) ASD-TDR-62-542, Part IV, October 1963

7. D. D. Seath, Vibration of an Inflatable Fabric Wing Model, Dissertation for the Degree of Doctor of Philosophy, Iowa State University of Science and Technology, Ames, Iowa, 1963.

8. R. W. Leonard, G. W. Brooks, and H. G. McComb, Jr., Structural Considerations of Inflatable Re-entry Vehicle, NASA TN D-457, September 1960.

9. H. G. McComb, Jr., A Linear Theory for Inflatable Plates of Arbitrary Shape, NASA TN D-930, October 1961.

10. W. H. Stroud, Experimental and Theoretical Deflections and Natural Frequencies of an Inflatable Fabric Plate, NASA TN D-931, October 1961.

11. J. B. Monfort, Inflatable Structure Test Program, AFFDL-TR-65-181 December 1965.

12. A. F. Foerster, et al, Analytical and Experimental Investigation of Coated Metal Fabric Expandable Structures for Aerospace Applications, ASD-TDR-63-542, November 1963.

13. R. L. Bisplinghoff, H. Ashley, and R. L. Halfman, Aeroelasticity, Addison-Wesley Publishing Company, Inc., Reading, Massachusetts, 2nd Printing, November 1957.

14. R. I. Scoville, A. D. Topping and R. W. Nordlie, Model Data, Inflatable Model for Dynamic Thermoelastic Tests, GER-11740, 1964.

15. R. W. Nordlie, Model Data, Inflatable Model for Dynamic Thermoelastic Tests, GER-11740, Supplement 1, 1965.

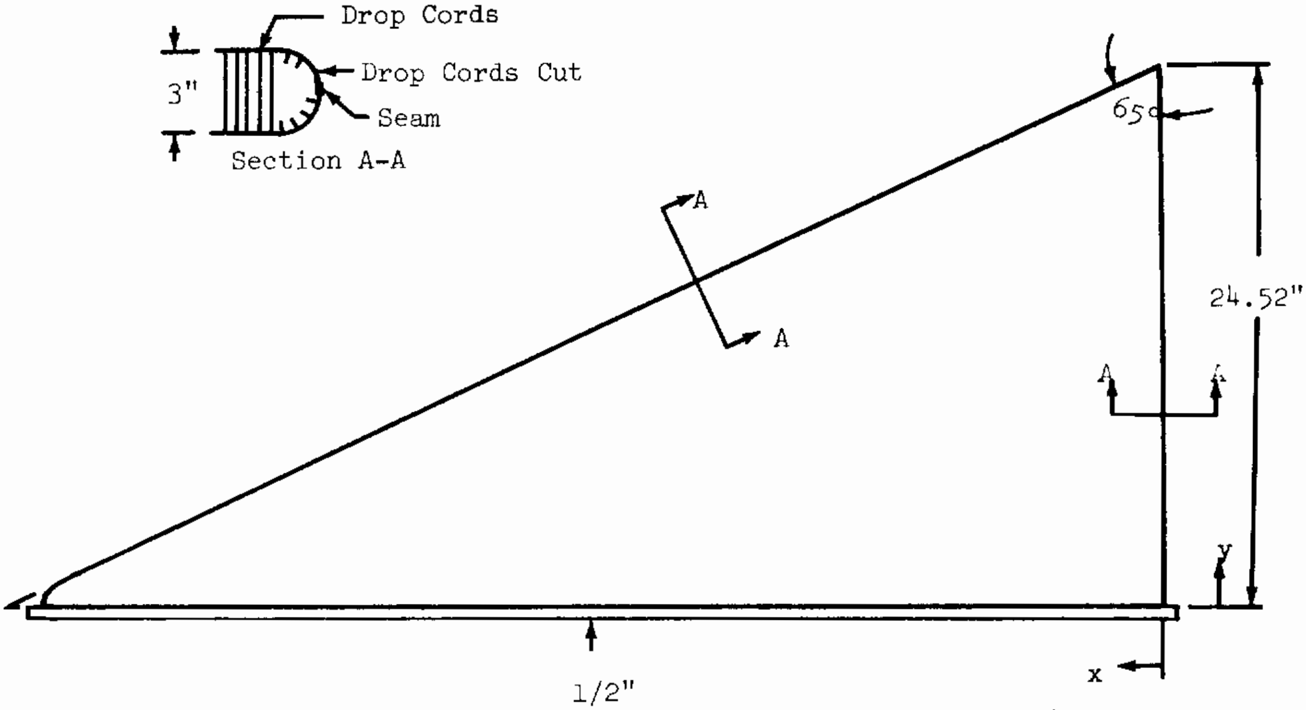

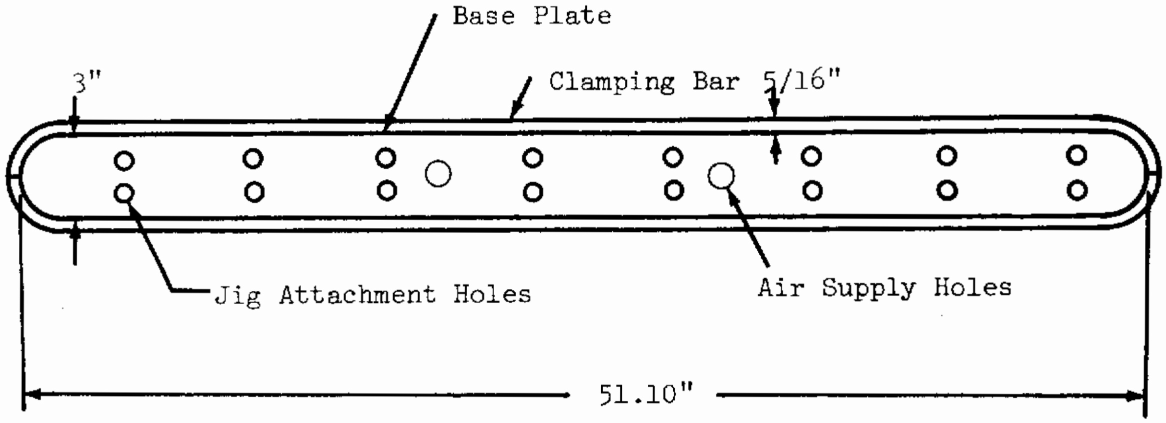

Figure 1 - Inflatable Delta Wing Model and Base Plate

Figure 2 - Model One in Test Jig Showing Location of Load Deflection Points on Upper Surface

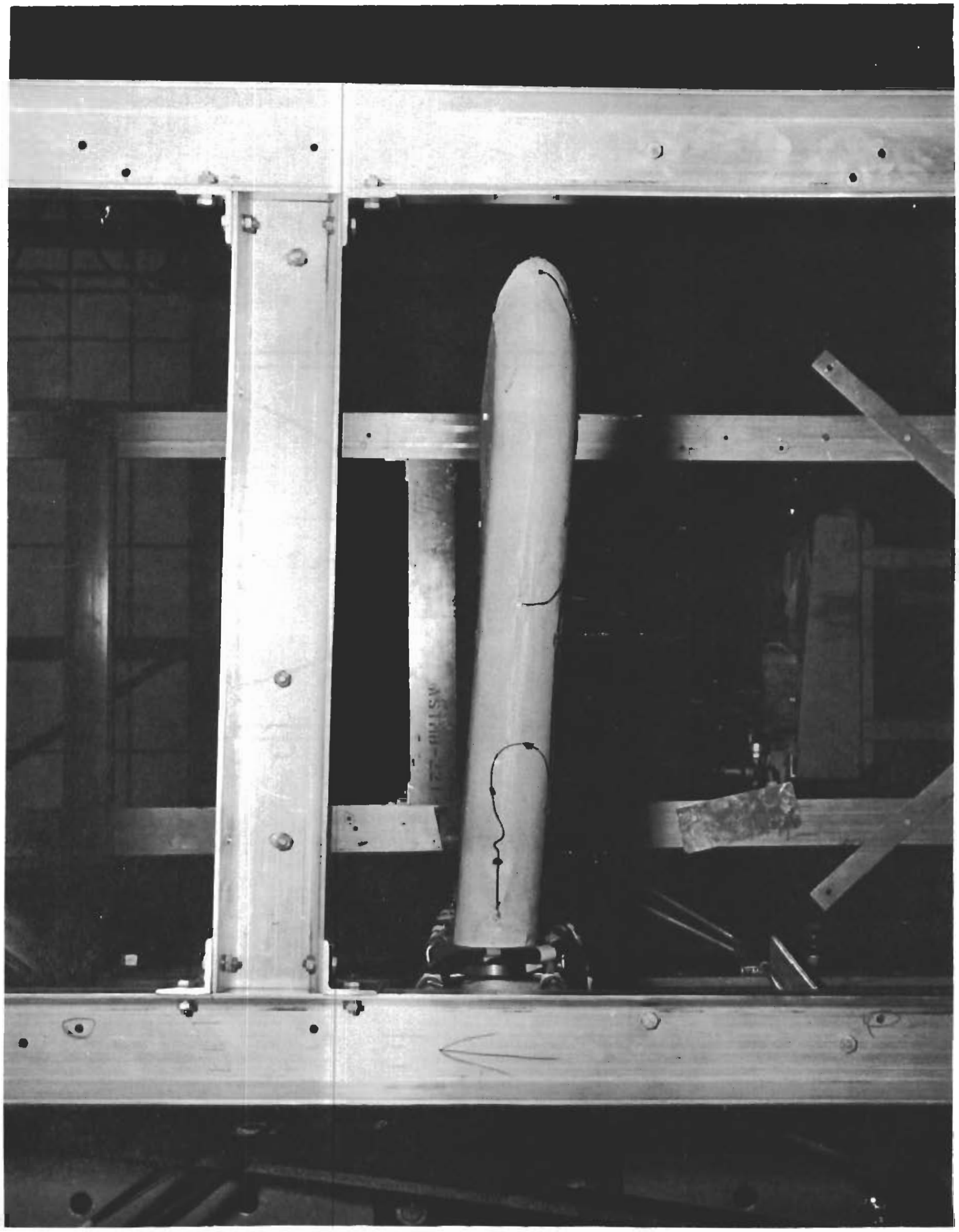

Figure 3 - Trailing Edge of Model One in the Test Jig

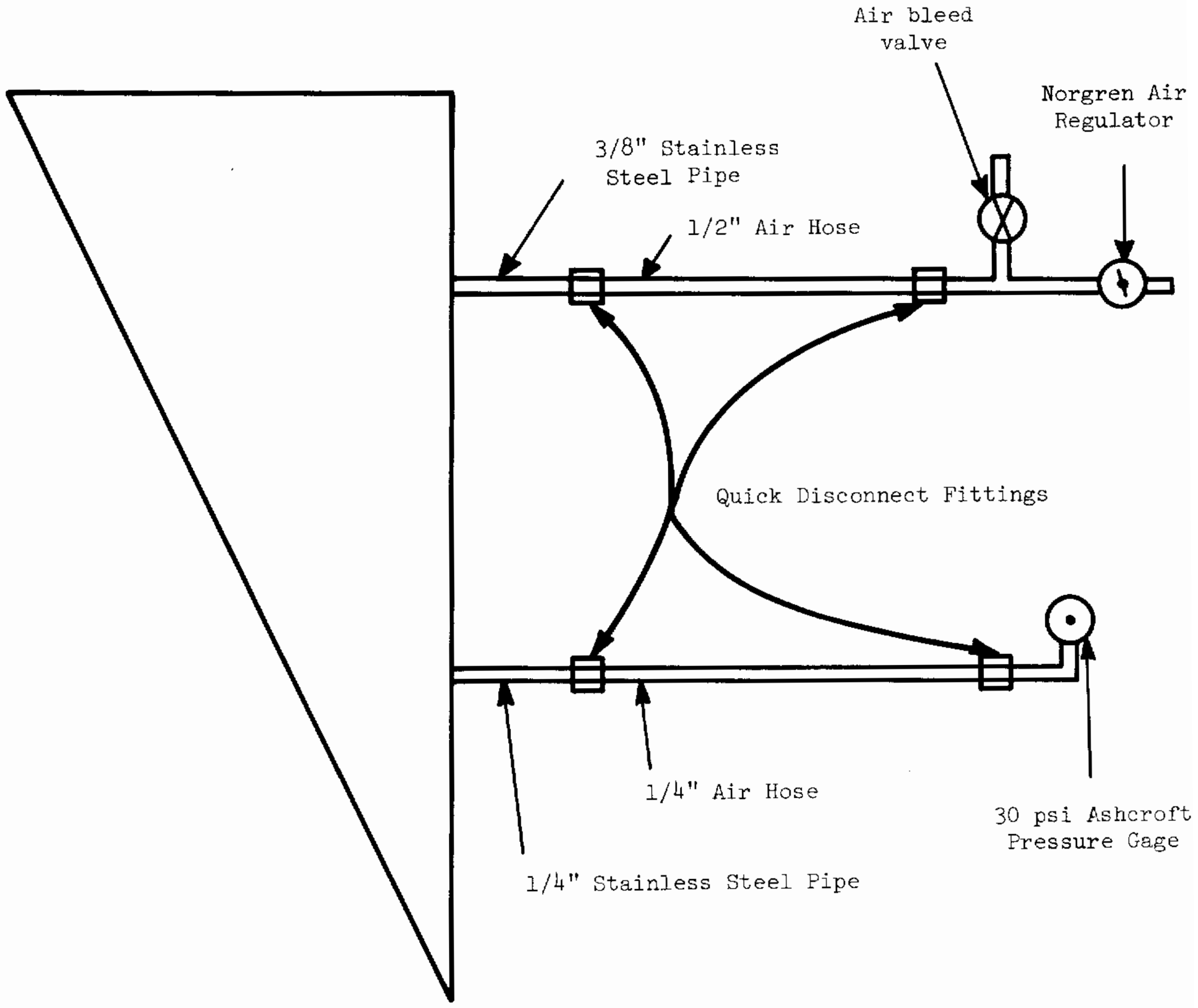

Figure 4 - Pressurization Equipment Schematic

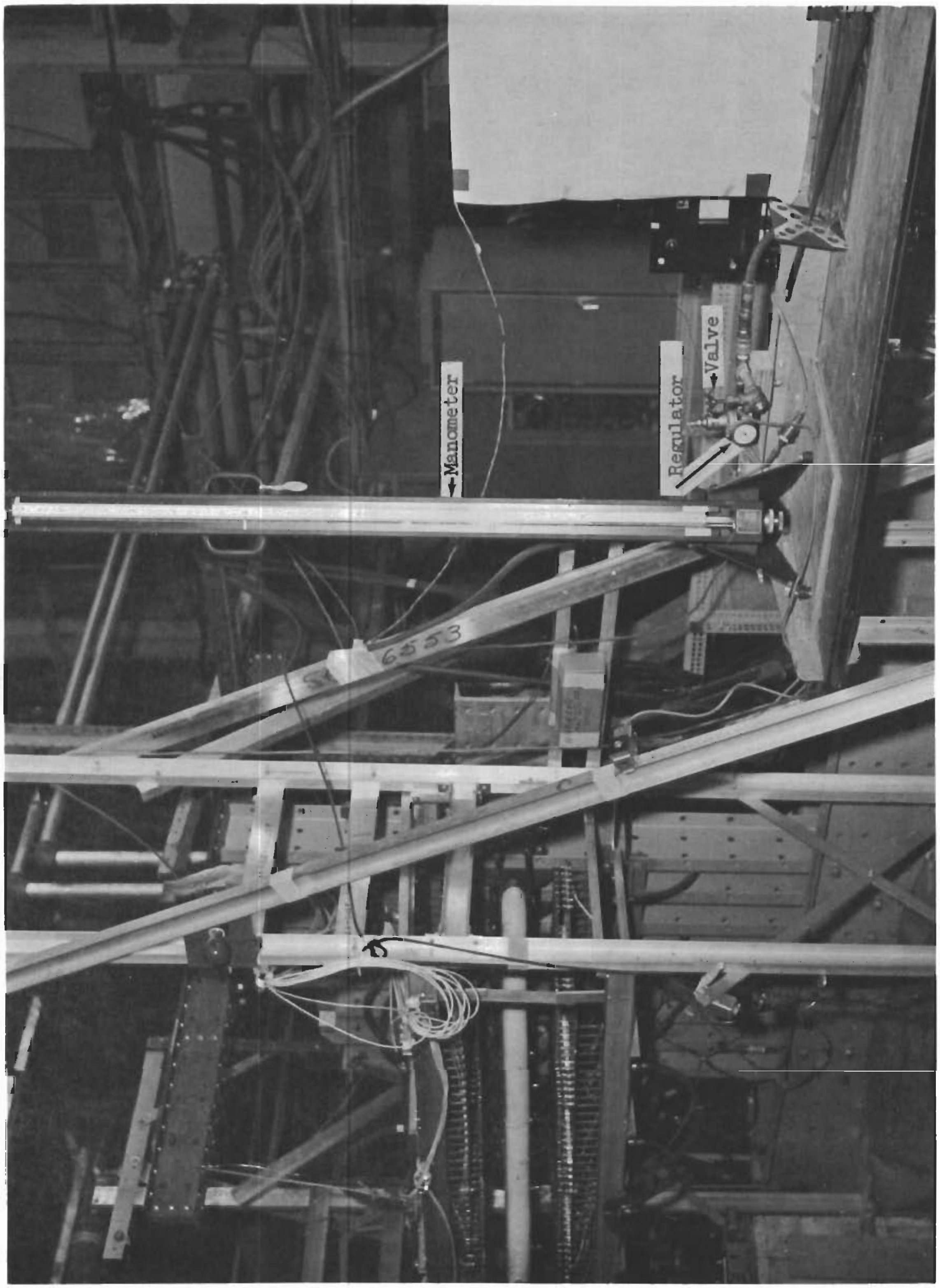

Figure 5 - Pressurization Equipment

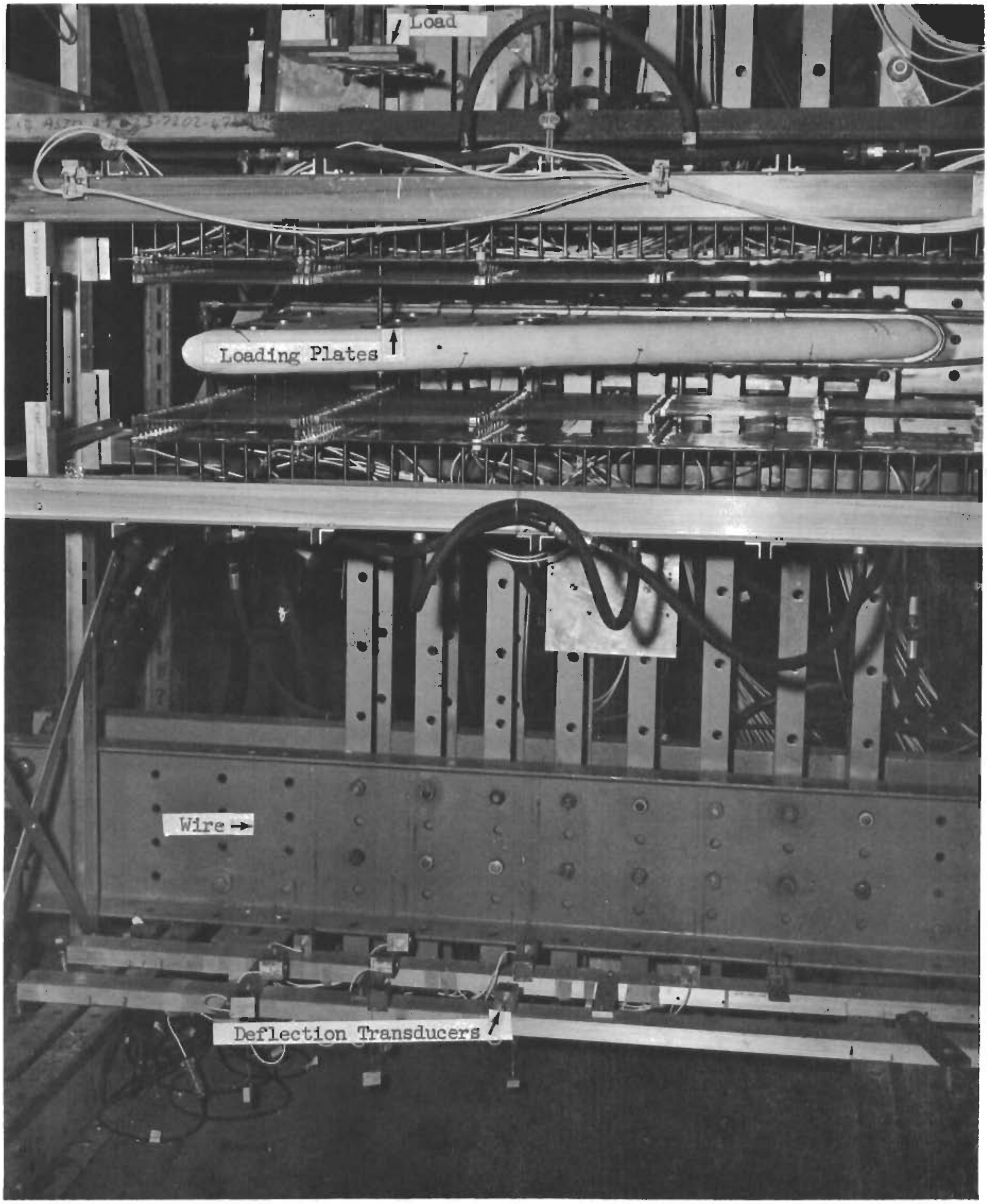

Figure 6 - Model Two Demonstrating Test Procedures for Determining Influence Coefficients

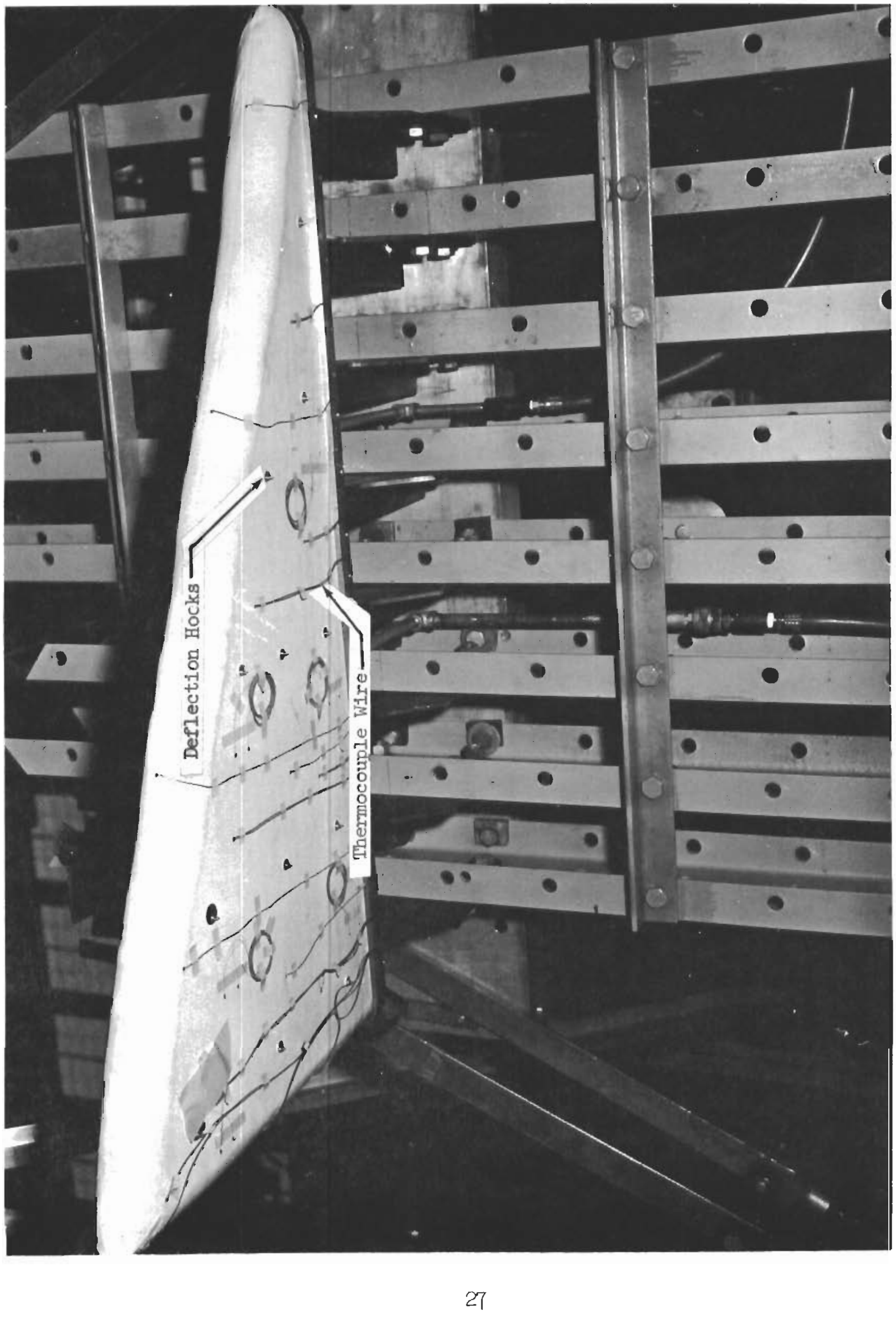

Figure 7 - Model One in Test Jig Showing Location of Load Measurement Points On Lower Surface

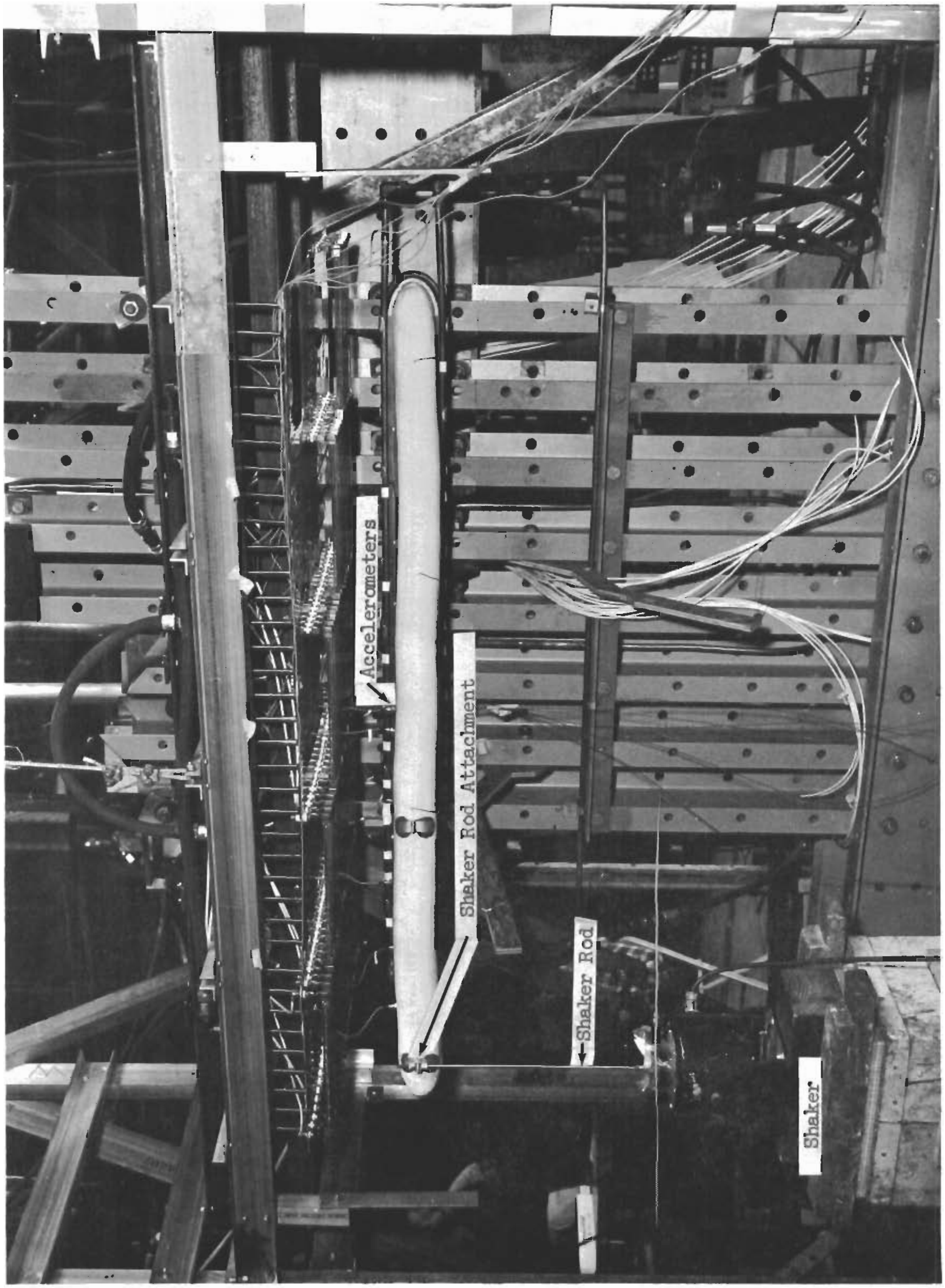

Figure 8 - Vibration Test Setup for Model One

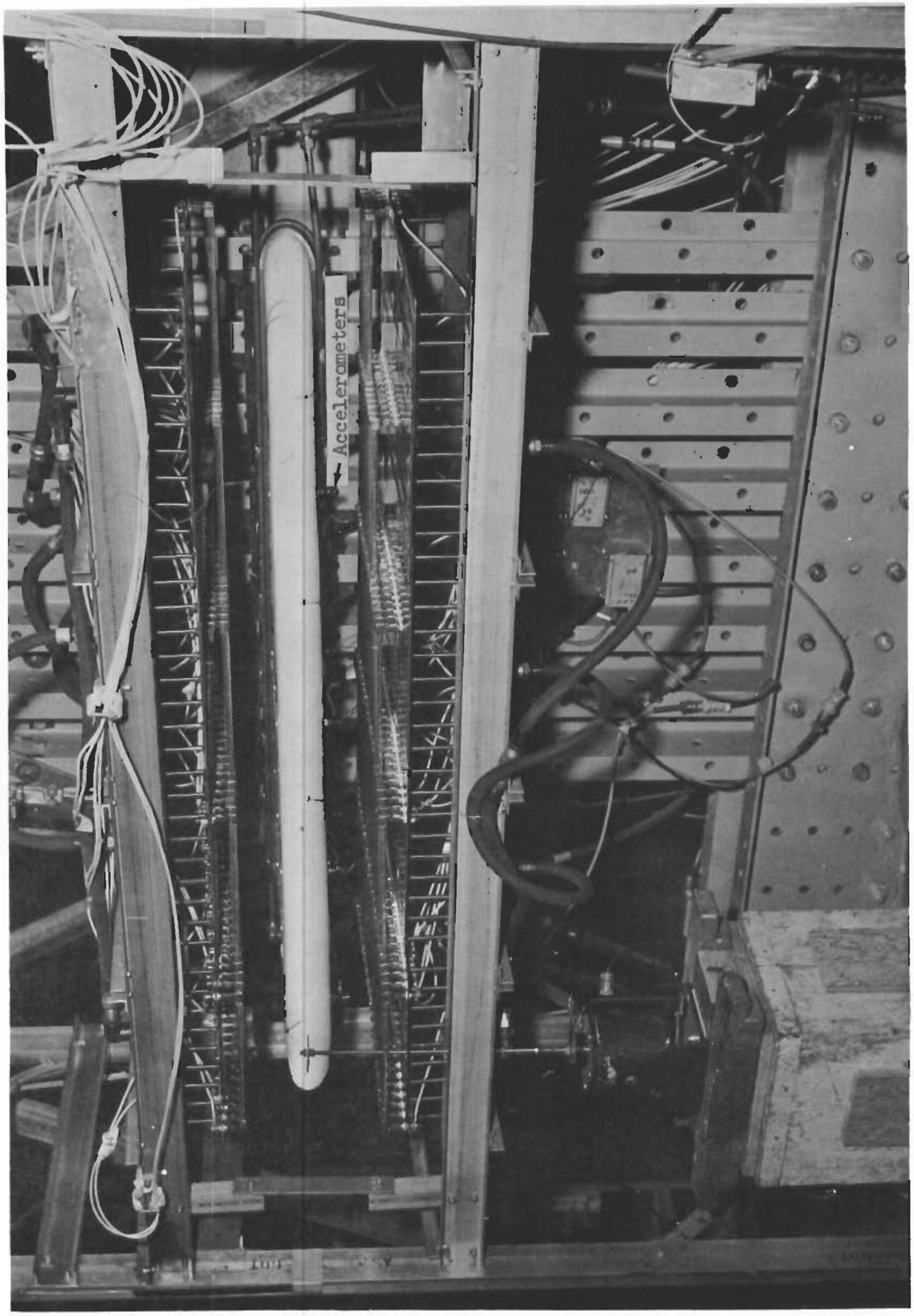

Figure 9 - Vibration Test Setup for Model Two

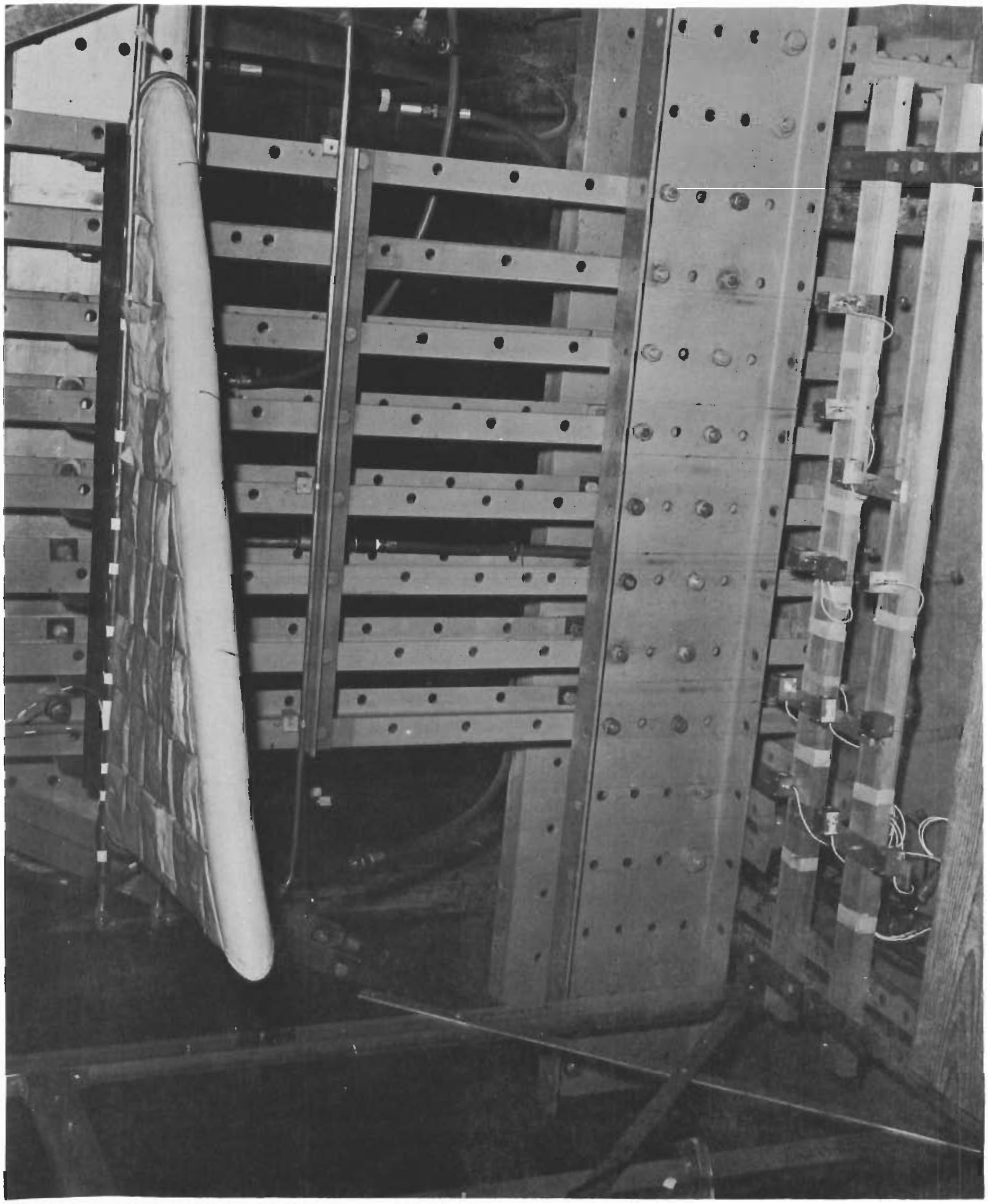

Figure 10 - Model One with a 20 Pound Distributed Load and Internal Pressure of 2 psi

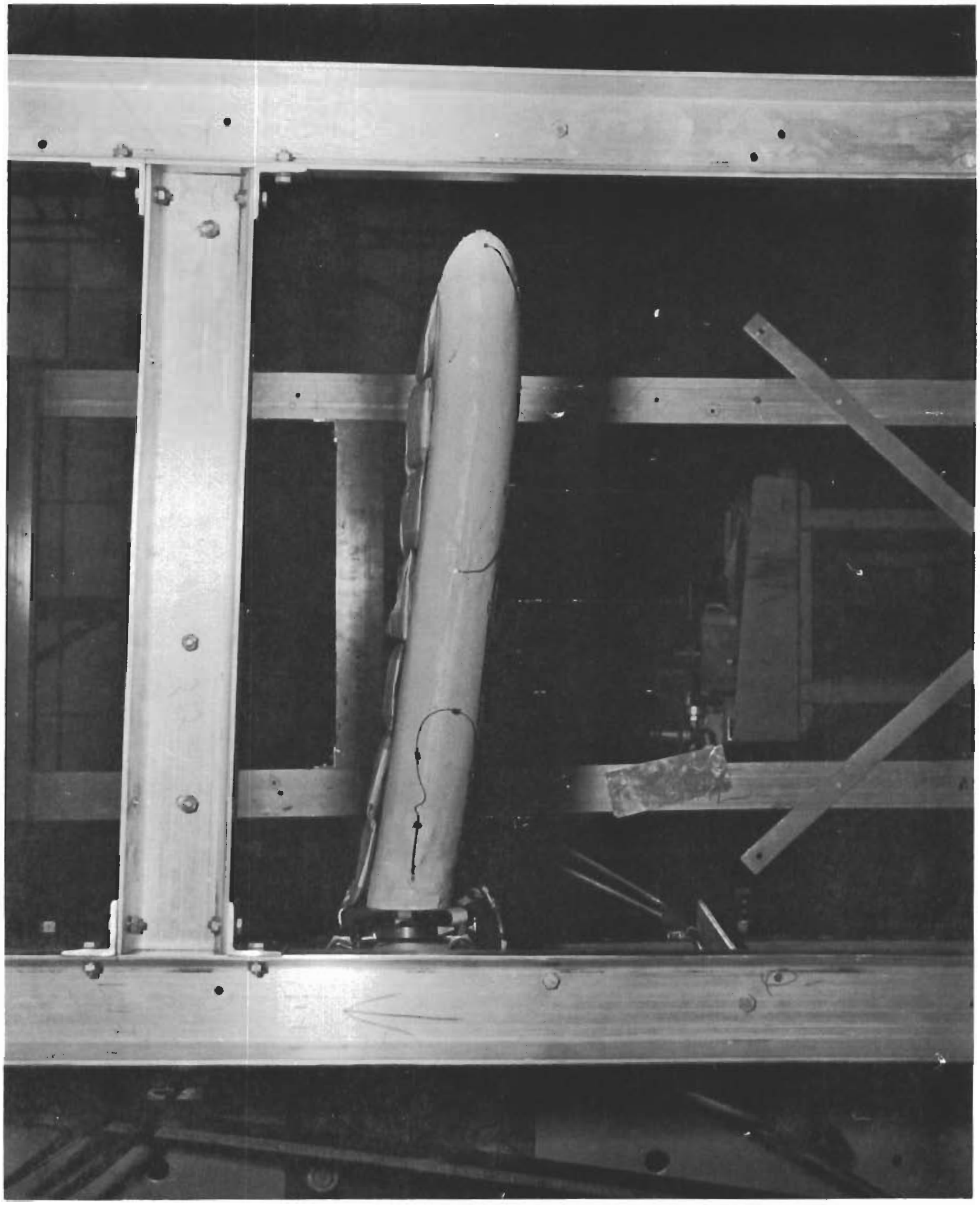

Figure 11 - Trailing Edge of Model One with a 20 Pound Distributed Load and Internal Pressure of 2 psi

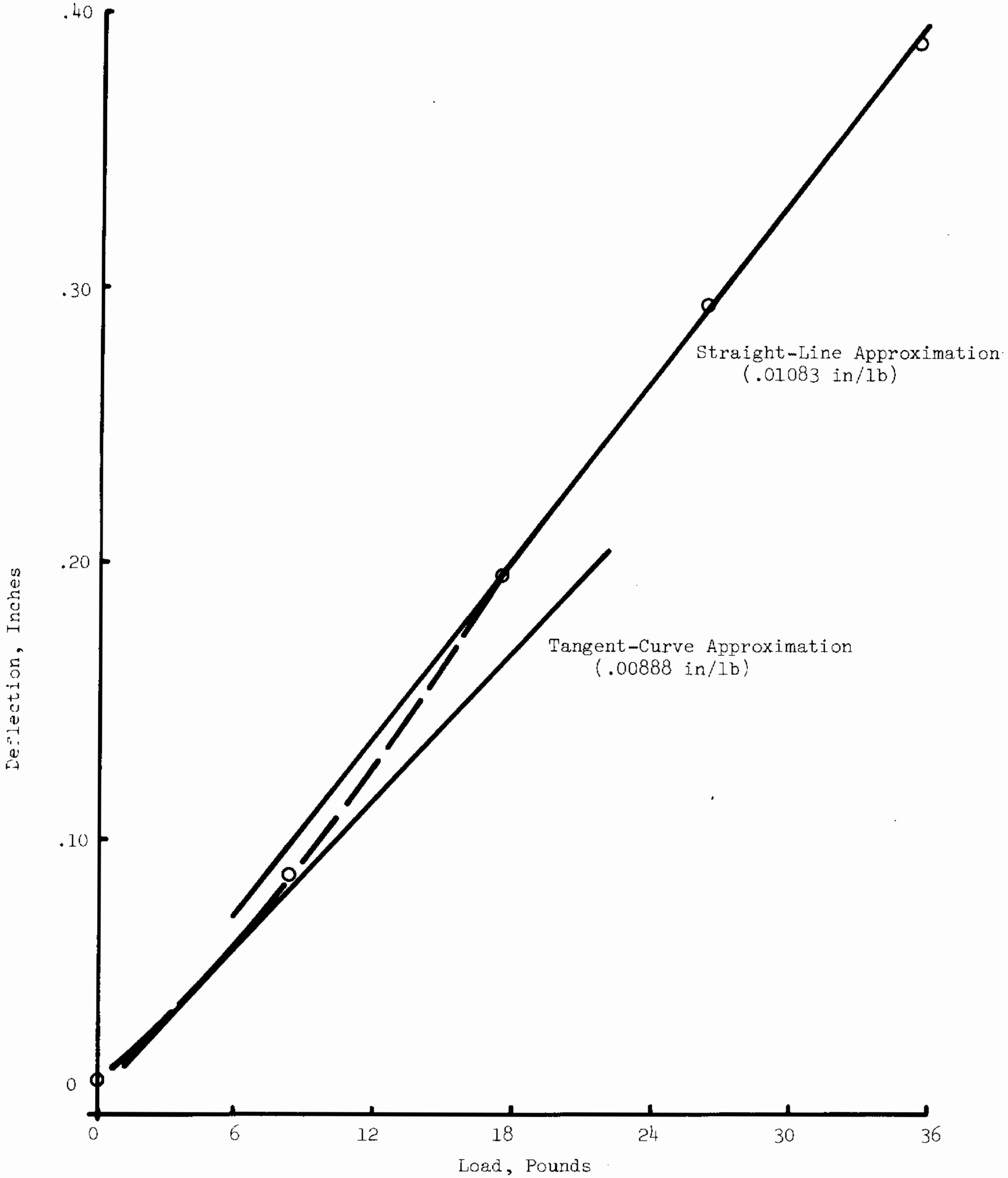

Figure 12 - Typical Room Temperature Flexibility Influence Coefficient Plot, Deflection at Point 37 with Load at Point 37, 10 psi

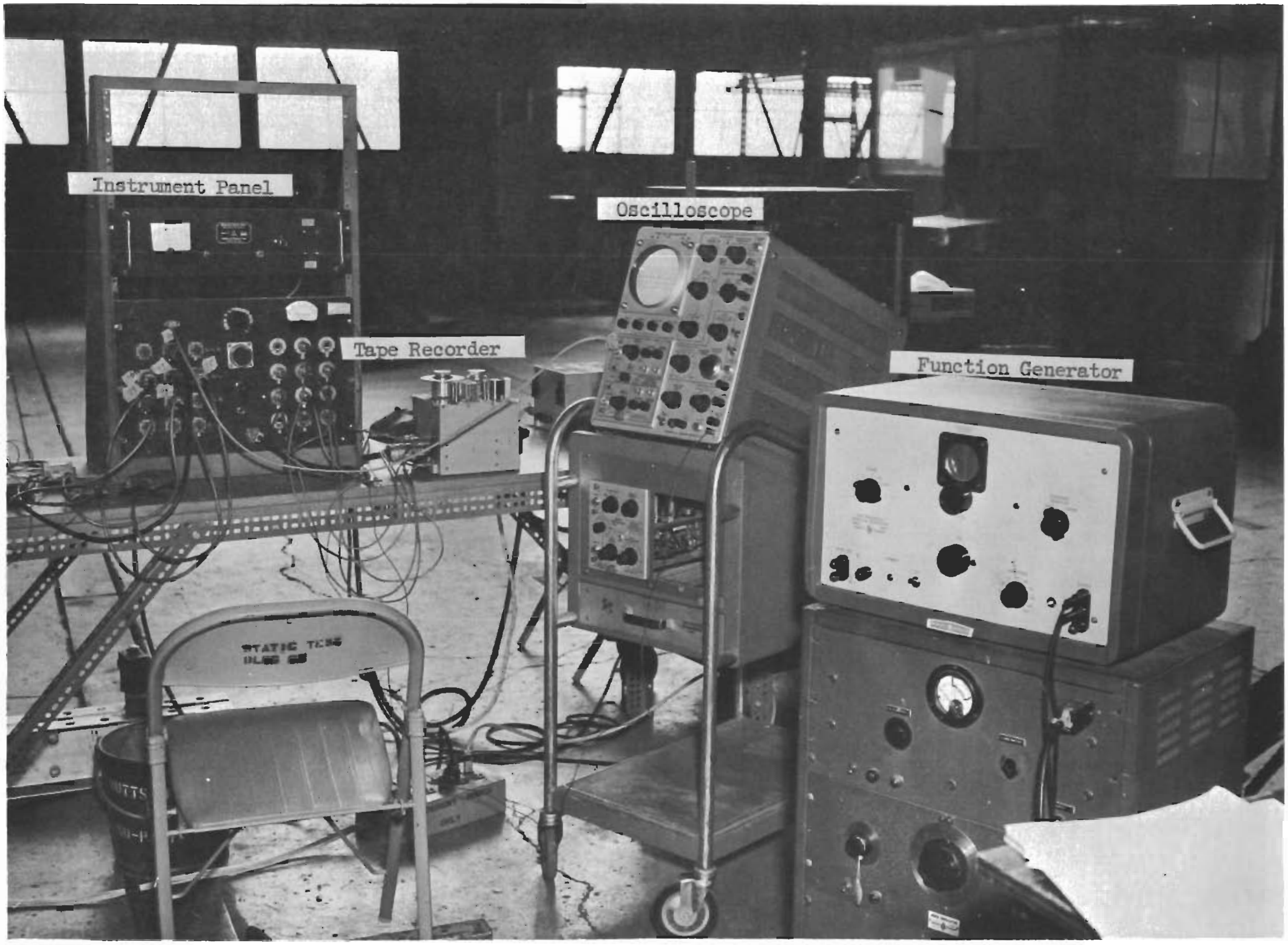

Figure 13 - Vibration Test Equipment for Model One

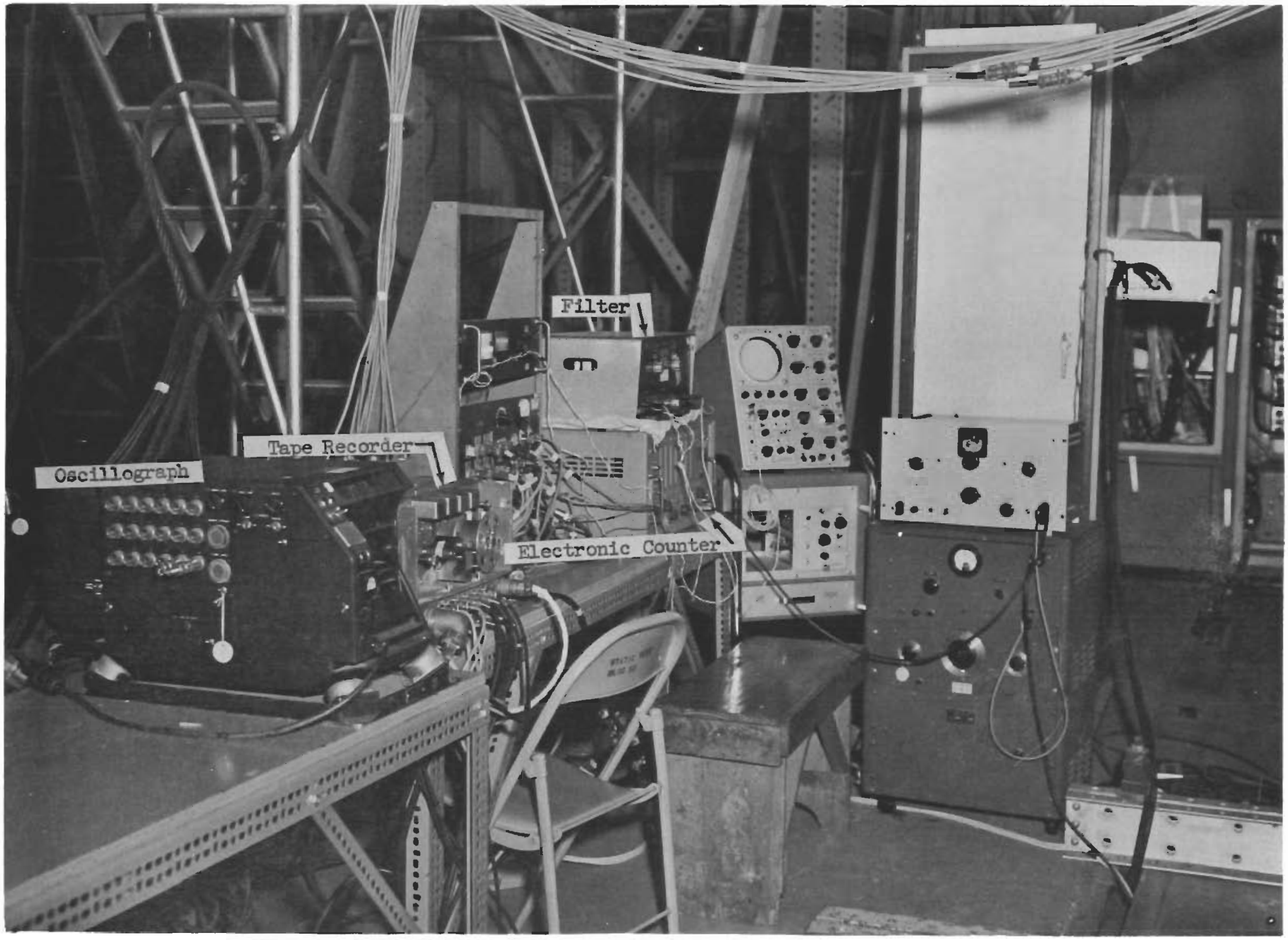

Figure 14 - Vibration Test Equipment for Model Two

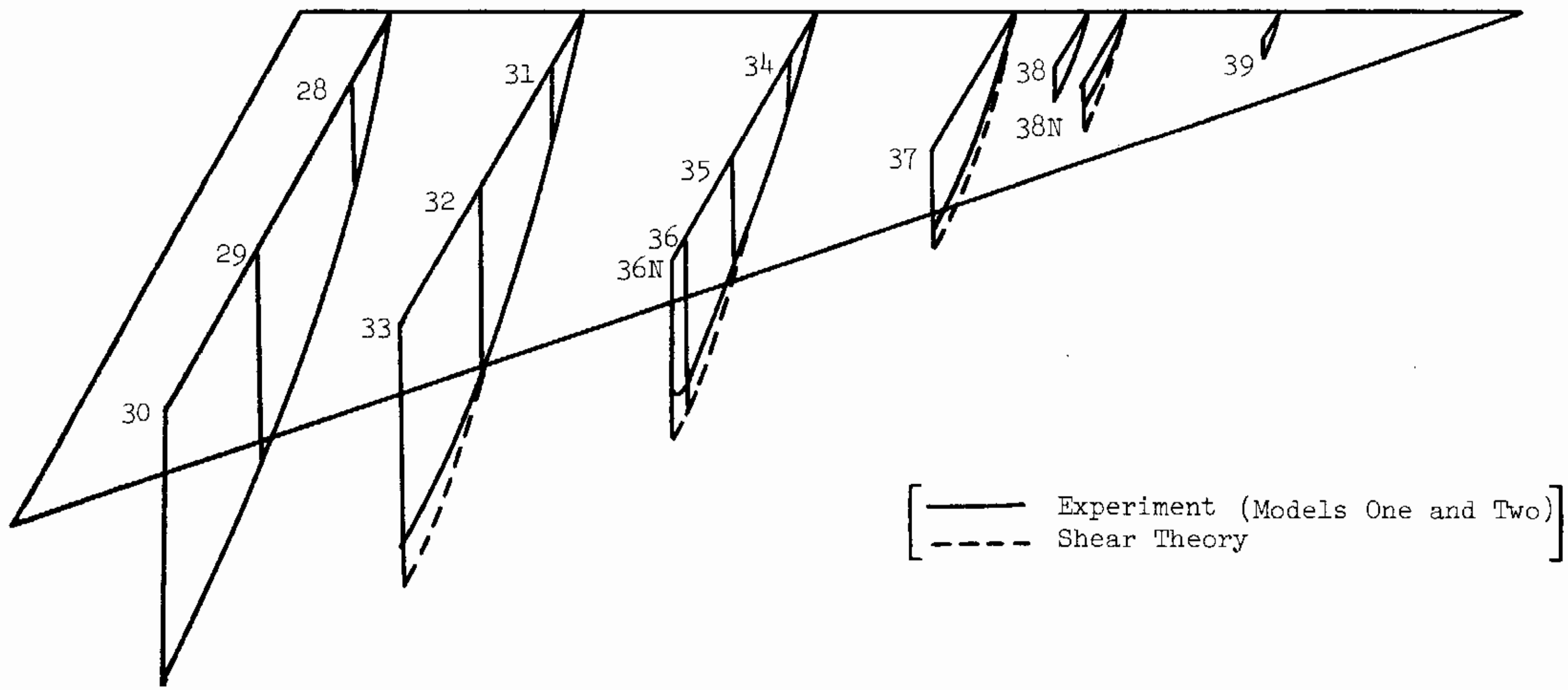

Figure 15 - Comparison of Experimental and Shear Theory Predicted Deflections for Models One and Two with a Total Load of 20 Pounds Uniformly Distributed and an Internal Pressure of 2 psi

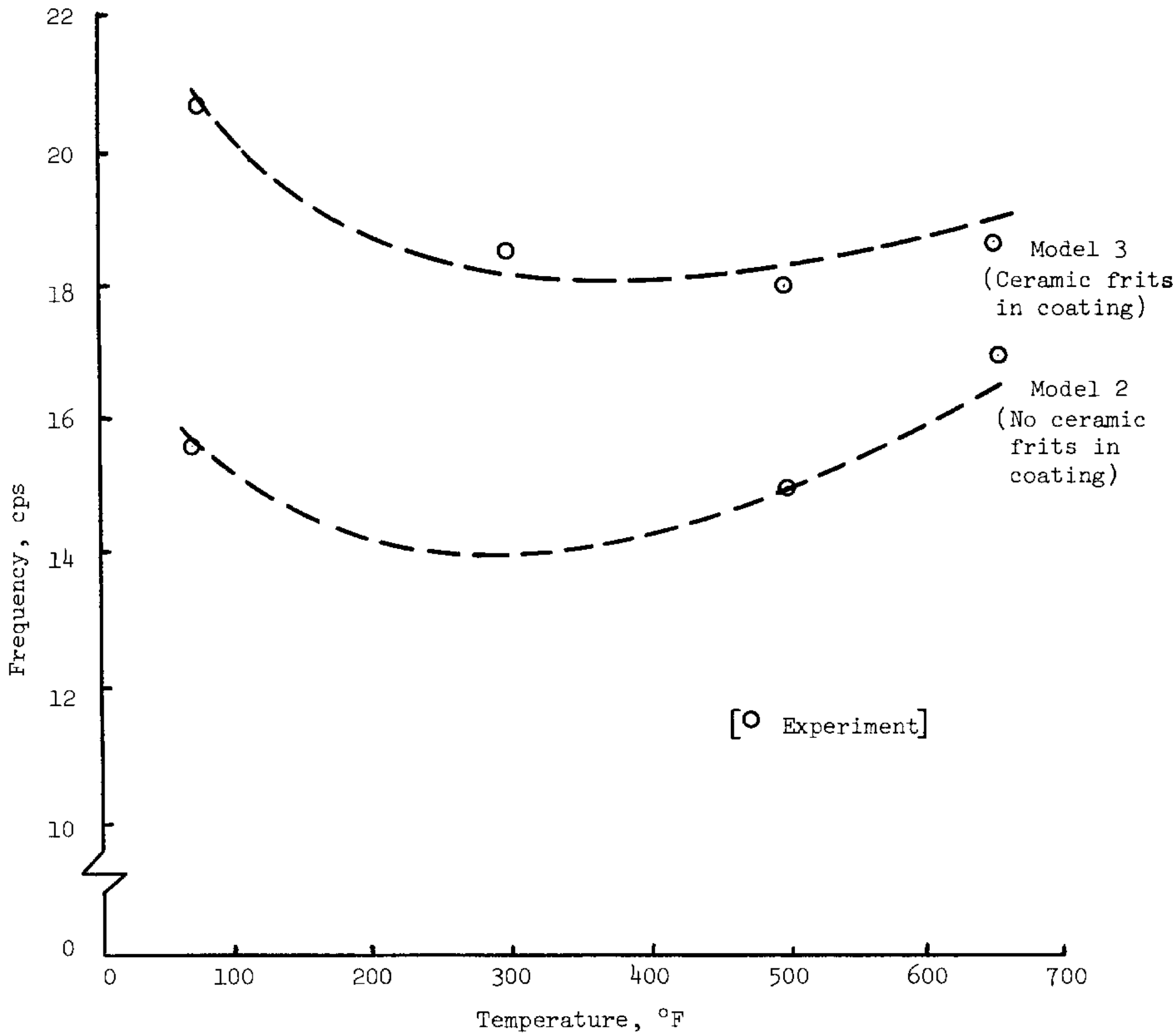

Figure 16 - Effect of Temperature on the First Vibration Mode Frequency at 10 psi

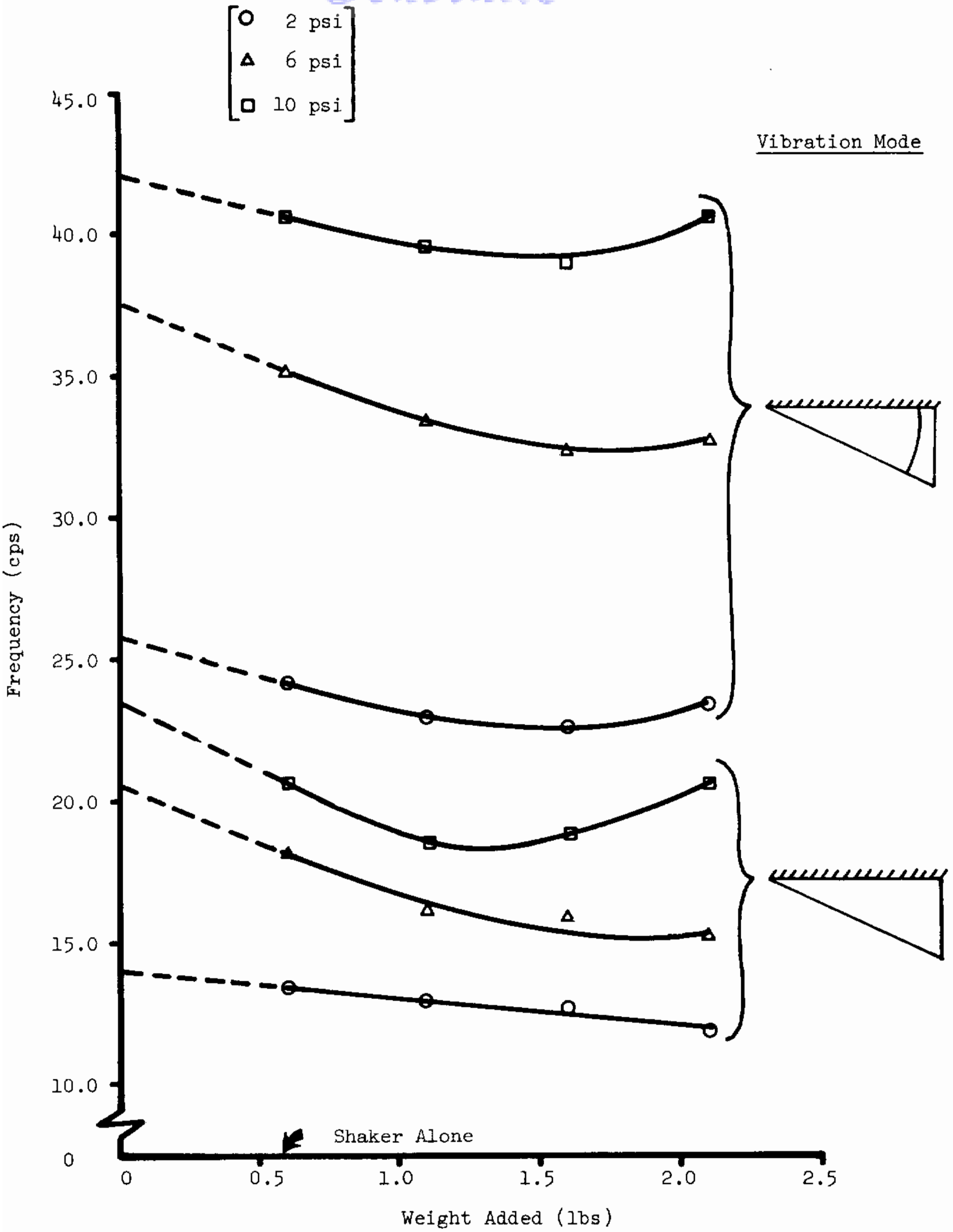

Figure 17 - Experimental Effect on the Natural Vibration Frequencies of Model Three from Additional Masses Attached to the Excitation Equipment

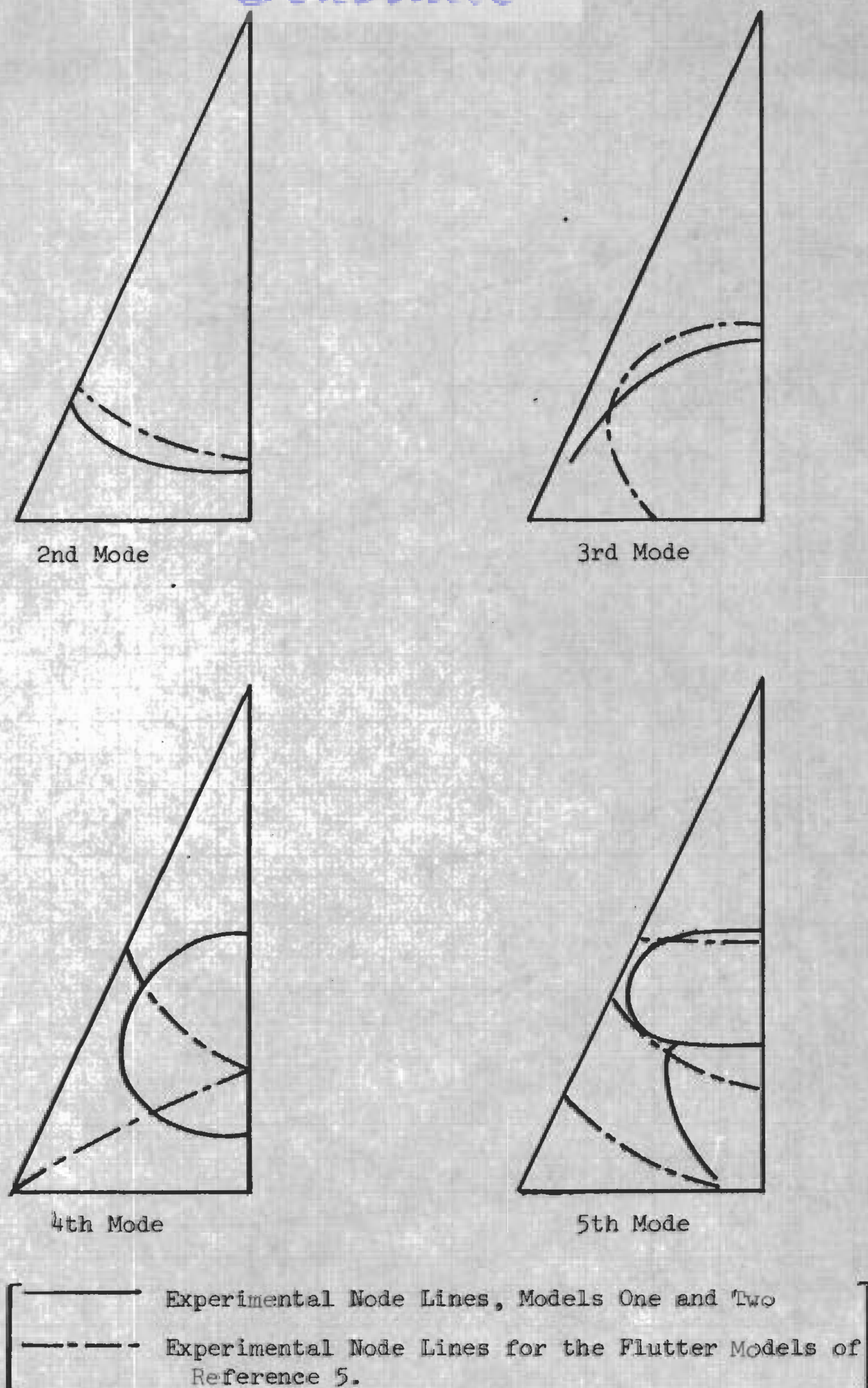

Figure 18 - Comparison of Experimental Node Lines with Those Reported for the Flutter Models of Reference 5

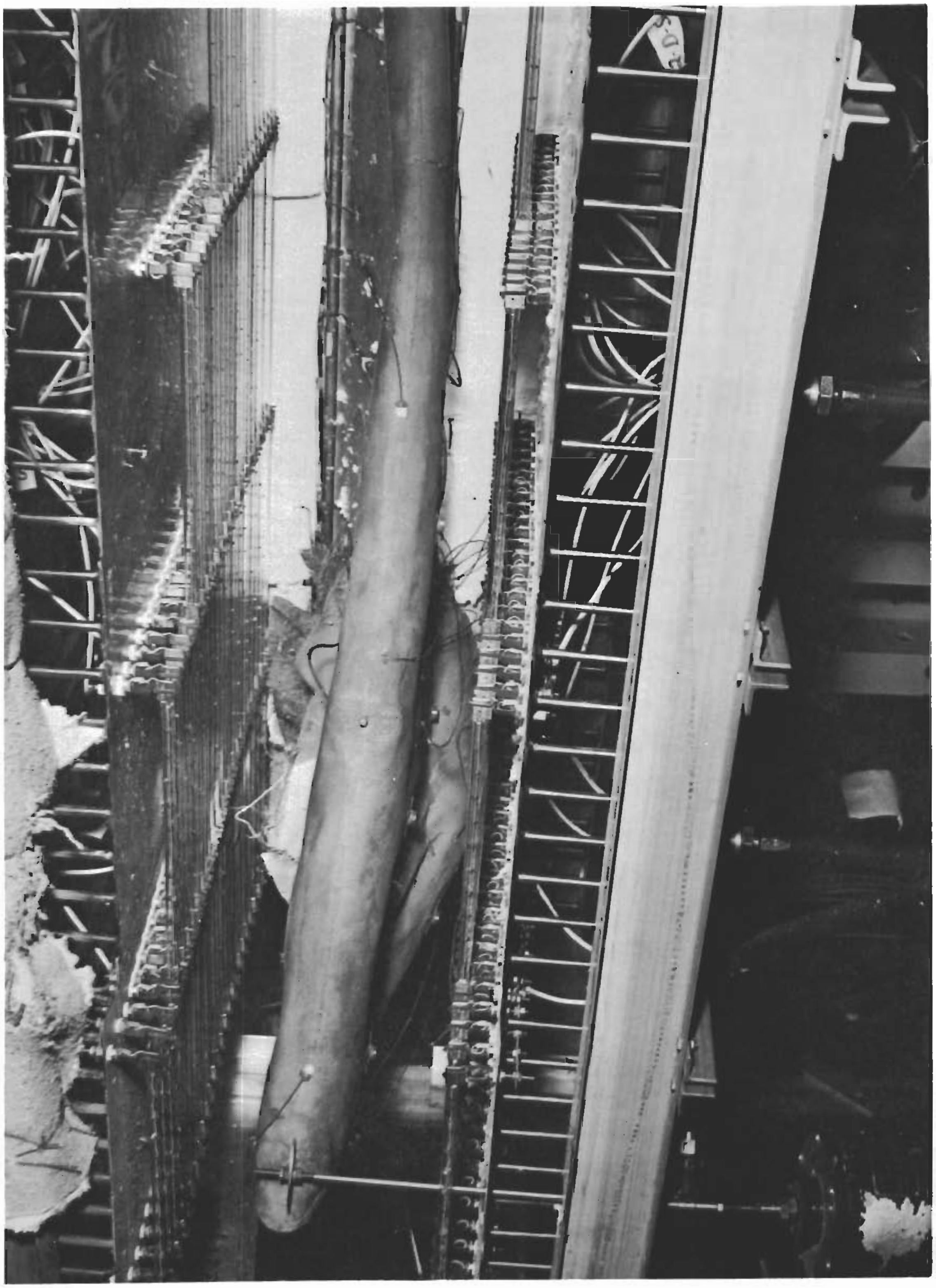

Figure 19 - Model Three After Failure During 800°F Vibration Test at 10 psi

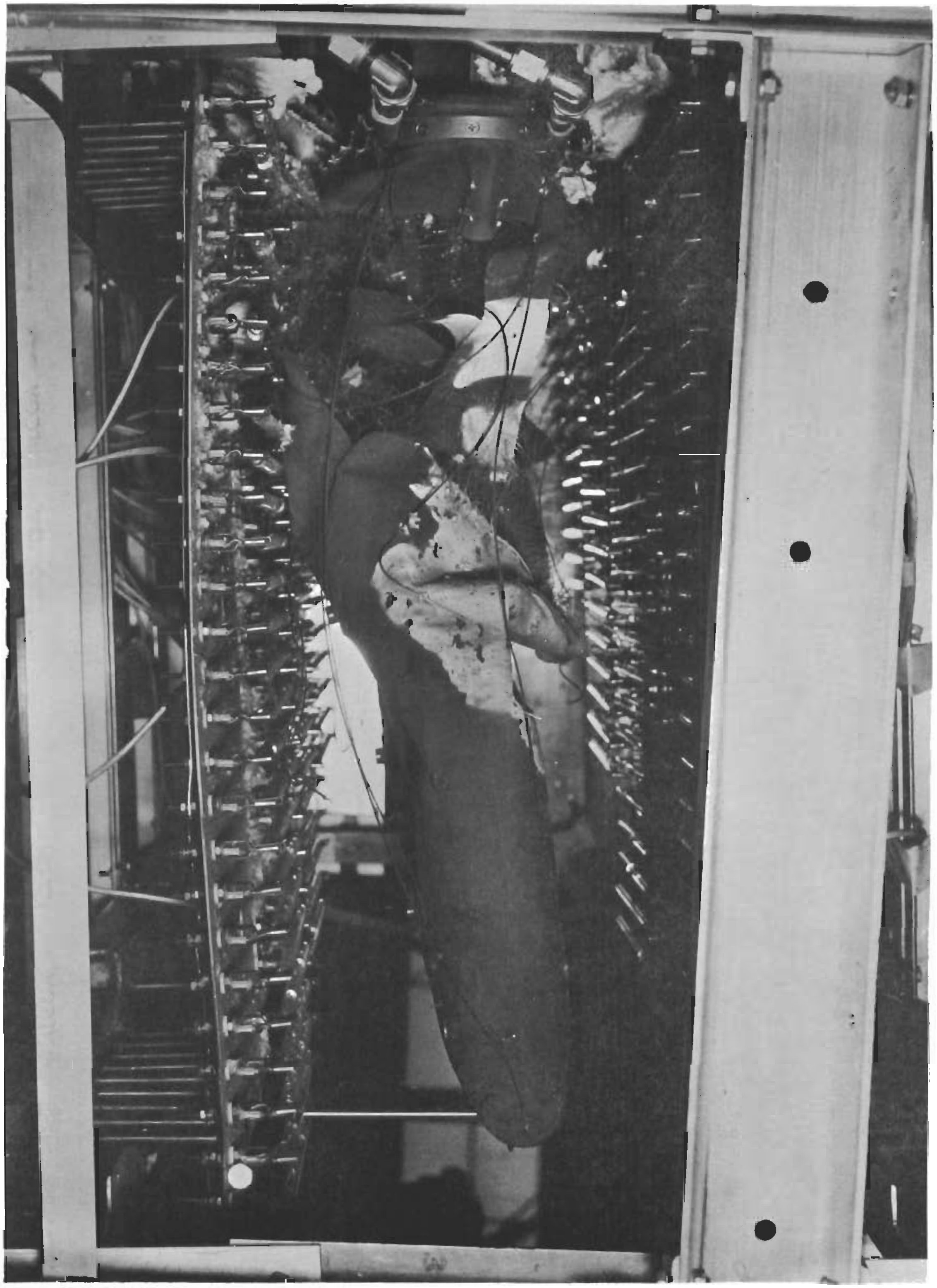

Figure 20 - Trailing Edge of Model Three After Failure During 800°F Vibration Test at 10 psi

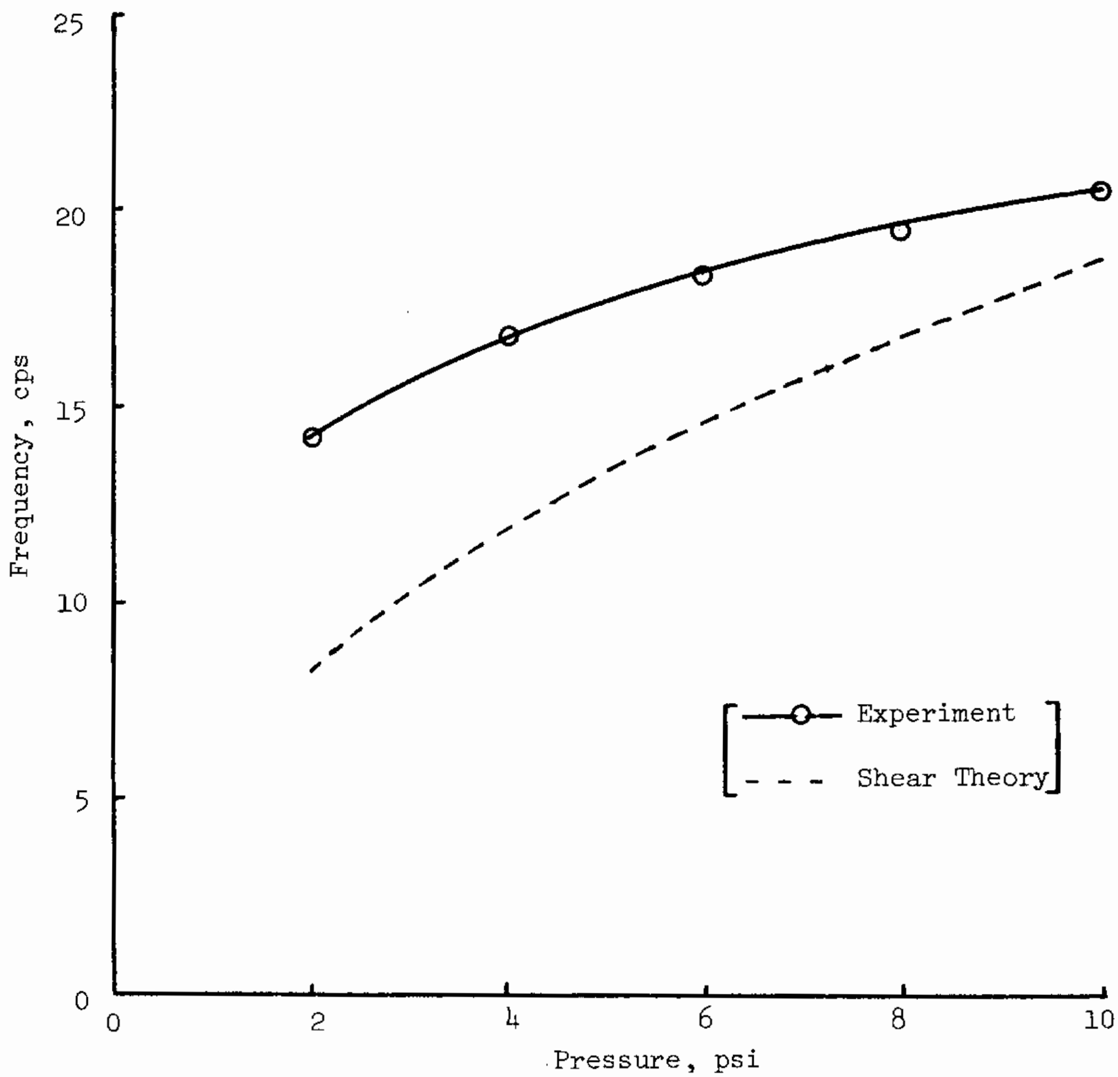

Figure 21 - Comparison of Predicted and Measured First Vibration Mode Frequency for Model Three

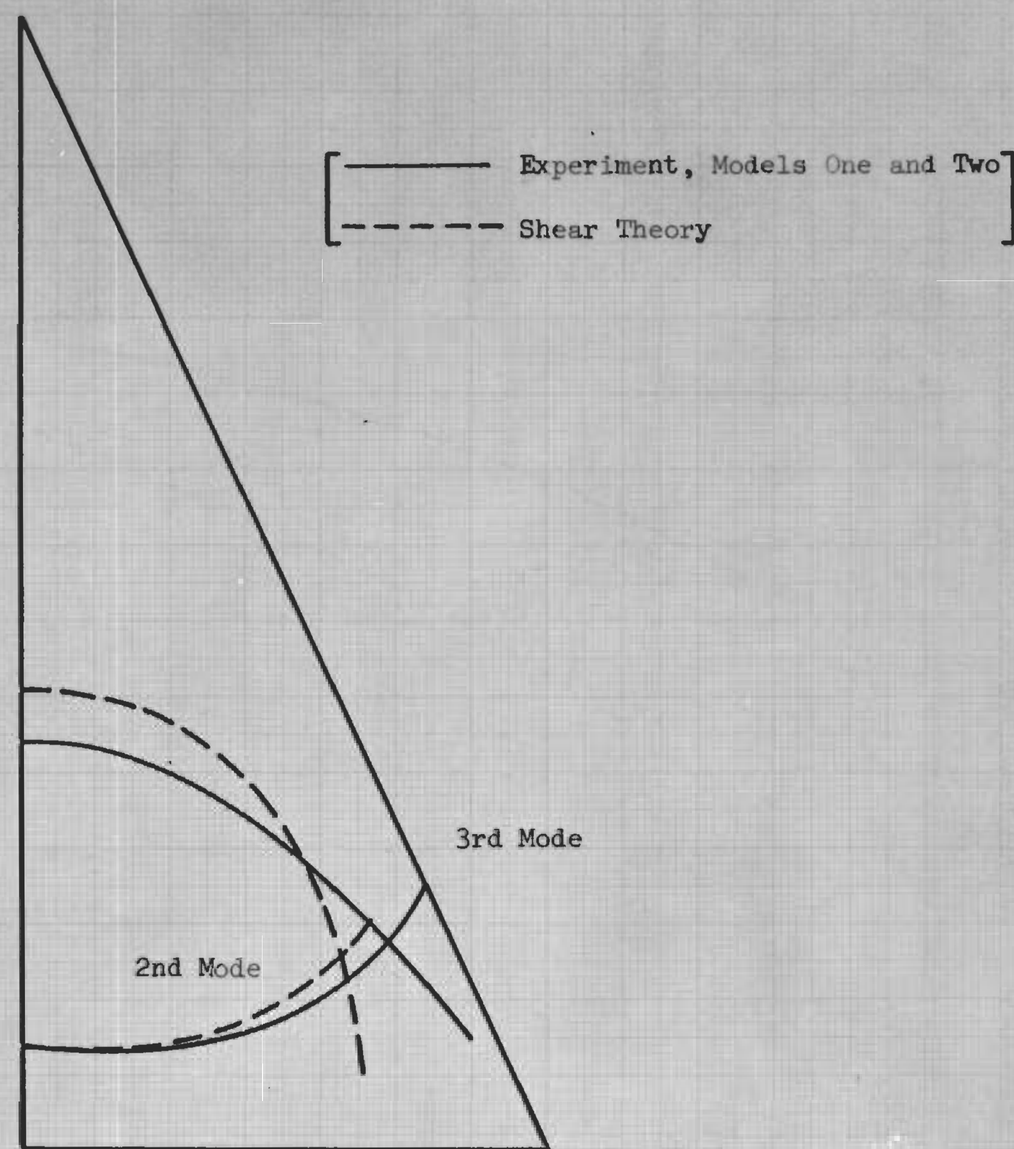

Figure 22 - Comparison of Node Lines for the Second and Third Modes from Shear Theory Predictions with Experiment

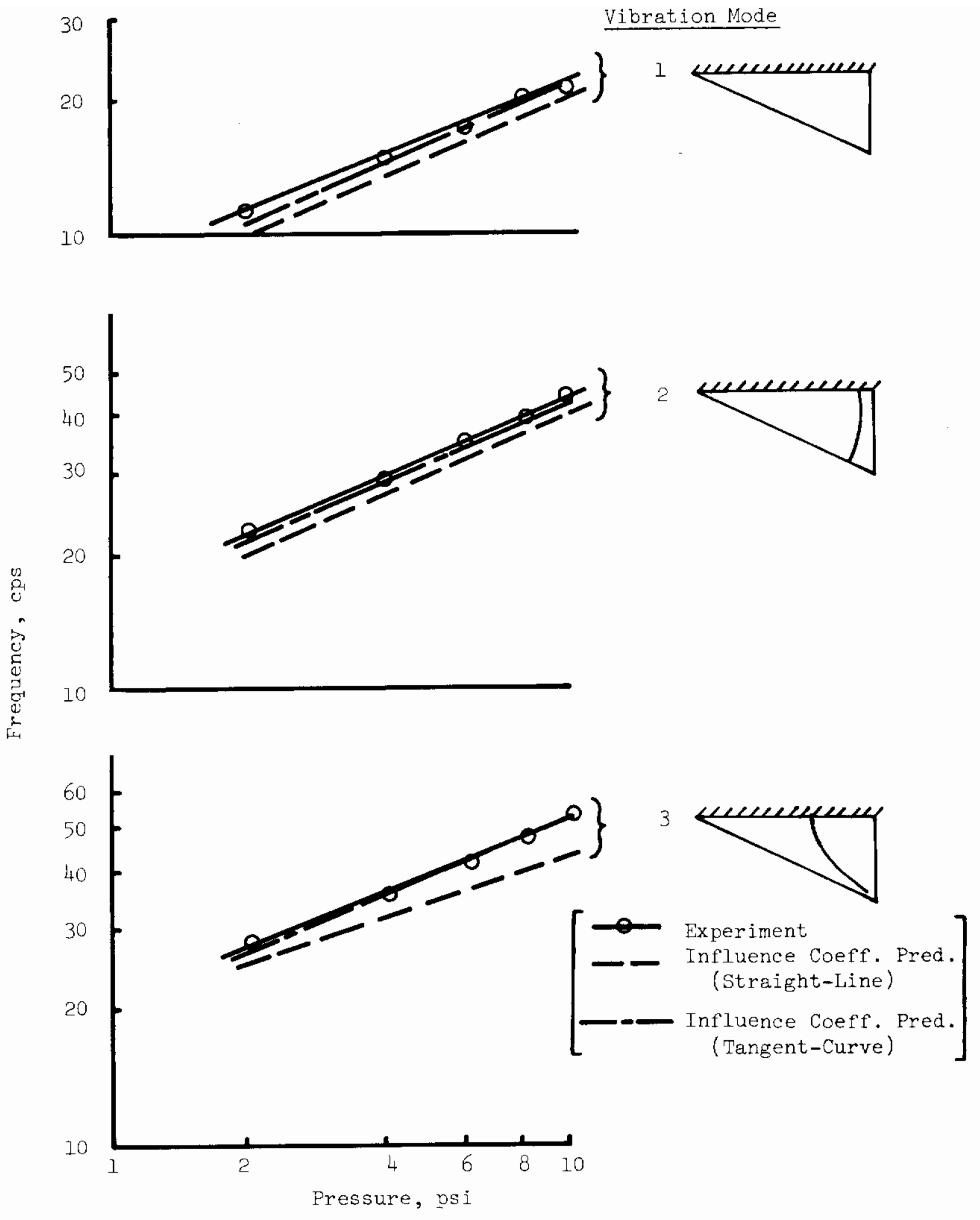

Figure 23 - Room Temperature Vibration Frequencies vs Pressure for Model One

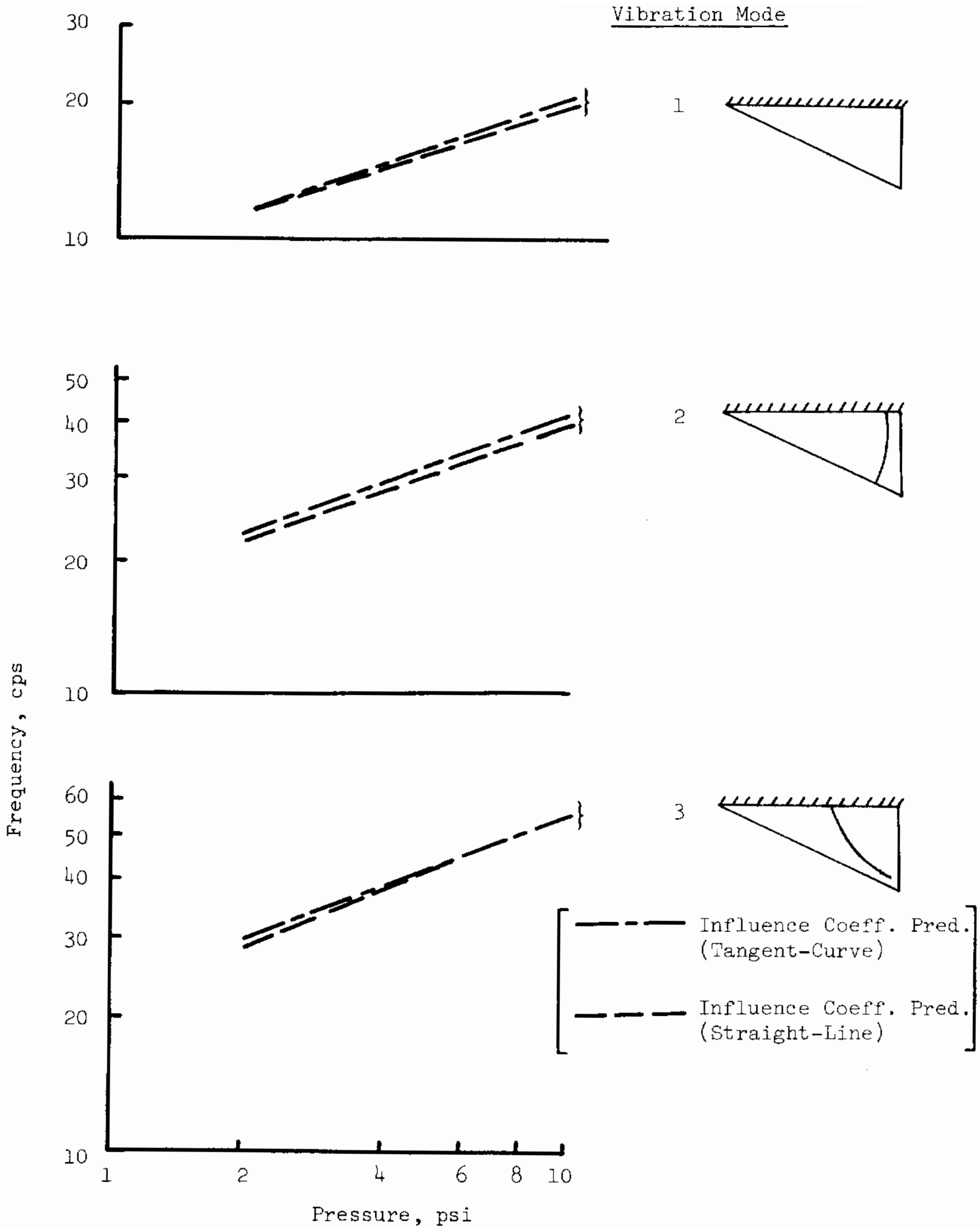

Figure 24 - Calculated Vibration Frequencies vs Pressure for Model One Based on Influence Coefficients Measured at 650°F

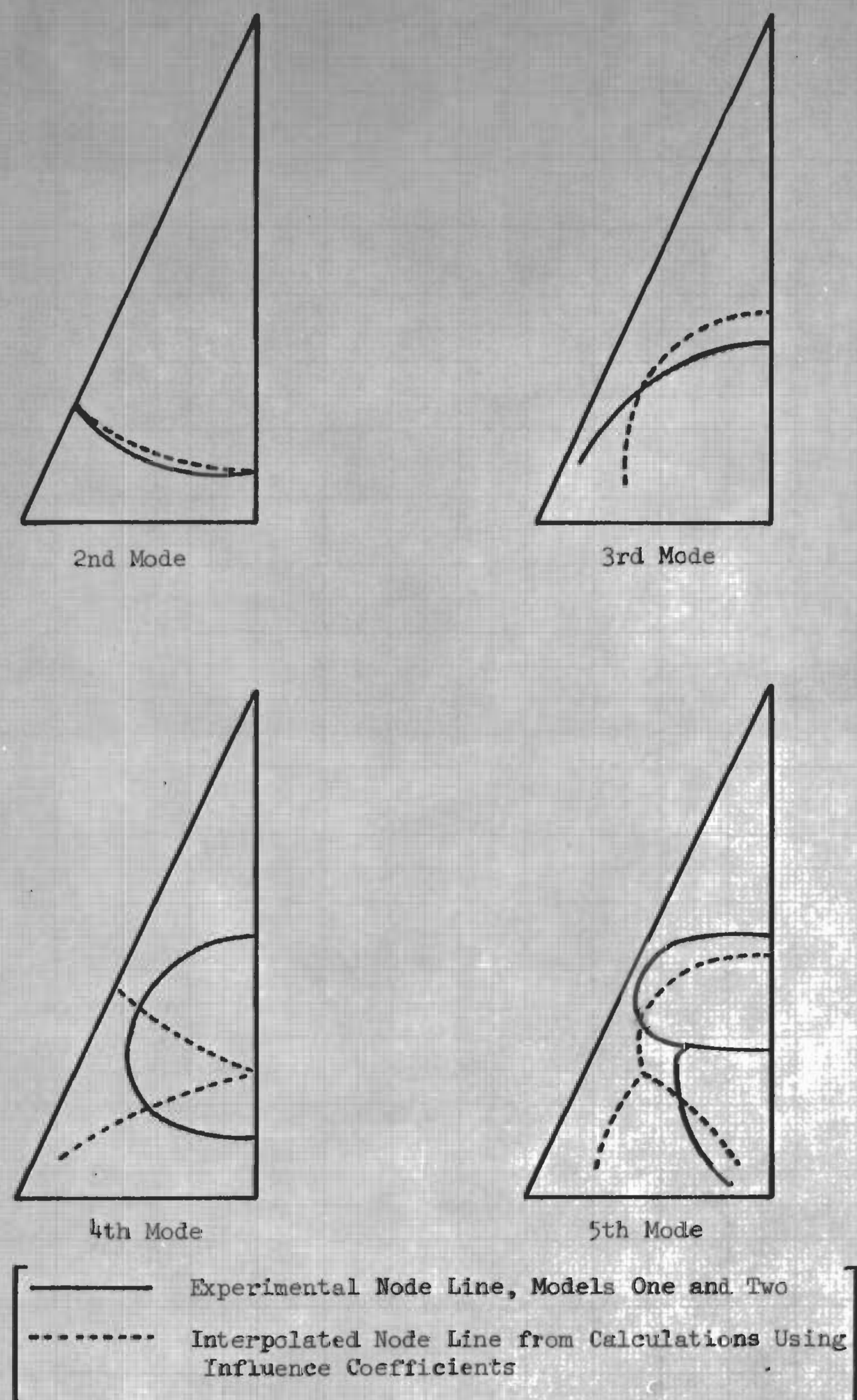

Figure 25 - Comparison of Node Lines Interpolated from Vibration Calculations Using Influence Coefficients with Experiment

Table 1 - Location of Loading, Deflection Measuring, and Accelerometer Attachment Points

Point Number		Location	
Model One	Models Two and Three	x, inches	y, inches
28	28	3.75	3.00
29	29	3.75	11.00
30	30	3.75	19.00
31	31	11.84	2.50
32	32	11.84	8.50
33	33	11.84	15.50
34	34	21.56	2.00
35	35	21.56	7.00
36		21.56	11.00
37		29.65	7.00
38		32.89	2.50
39		40.99	1.50
	36N	21.56	12.00
	38N	34.51	3.50

Table 2 - Location of Thermocouples

Thermocouple No.	x, inches	y, inches	Model Surface
101	4.50	6.50	Top
201	4.50	6.50	Bottom
102	14.80	4.50	Top
202	14.80	4.50	Bottom
103	26.20	4.00	Top
203	26.20	4.00	Bottom
104	36.50	4.00	Top
204	36.50	4.00	Bottom
105	4.00	16.50	Top
205	4.00	16.50	Bottom
106	14.30	13.50	Top
206	14.30	13.50	Bottom
107	24.00	9.70	Top
207	24.00	9.70	Bottom
308	0	1.50	Center Line
109	8.50	1.50	Top
110	29.66	1.50	Top
311	46.06	-	Center Line
312	0	12.50	Center Line
313	0	24.92	Center Line
314	18.33	-	Center Line
315	32.90	-	Center Line
116	6.50	13.00	Top
117	15.84	10.50	Top
218	6.50	10.00	Bottom
219	15.84	7.50	Bottom
220	1.50	-	Bottom
221	10.10	-	Bottom
140	8.00	20.00	Top
141	19.00	15.00	Top
342	0	7.00	Center Line
343	0	18.75	Center Line
344	5.00	-	Center Line
345	26.20	-	Center Line

Table 3 - Vibration Frequency Predictions (cps) for Model One Based on Shear Theory of Reference 4

Mode	Frequency, cps				
	p = 2 psi	p = 4 psi	p = 6 psi	p = 8 psi	p = 10 psi
1	9.4	13.2	16.2	18.8	21.0
2	18.9	26.7	32.7	37.9	42.4
3	25.9	36.8	45.0	52.0	58.0

Table 4 - Vibration Frequency Predictions (cps) for Model Two Based on Shear Theory of Reference 4

Mode	Frequency, cps				
	p = 2 psi	p = 4 psi	p = 6 psi	p = 8 psi	p = 10 psi
1	8.6	12.0	14.8	17.1	19.1
2	17.2	24.2	29.8	34.4	38.5
3	23.6	31.4	41.0	47.4	52.9

Table 5 - Vibration Frequency Predictions (cps) for Model Three Based on Shear Theory of Reference 4

Mode	Frequency, cps				
	p = 2 psi	p = 4 psi	p = 6 psi	p = 8 psi	p = 10 psi
1	8.4	11.8	14.5	16.8	18.7
2	16.9	23.8	29.2	33.8	37.8
3	23.1	32.8	40.2	46.5	51.9

Table 6 - Predicted Uniform Load Deflections (Shear Theory - Reference 4)

Defl. Pt.	Vertical Deflection, w (x, y), inches					
	p=2 psi q=20 lbs	p=4 psi q=30 lbs	p=6 psi q=50lbs	p=8 psi q=60 lbs	p=10 psi q=80 lbs	p=10 psi q=60 lbs
28	.262	.197	.218	.197	.210	.157
29	.754	.566	.628	.566	.603	.452
30	.989	.742	.824	.742	.791	.593
31	.206	.155	.172	.155	.165	.124
32	.584	.438	.486	.438	.467	.350
33	.831	.623	.692	.623	.665	.499
34	.143	.107	.119	.107	.114	.086
35	.415	.311	.346	.311	.332	.249
36	.553	.415	.461	.415	.442	.332
37	.308	.231	.257	.231	.246	.185
38	.119	.089	.099	.089	.095	.071
39	.045	.034	.037	.034	.036	.027
36N	.578	.434	.481	.434	.462	.347
38N	.144	.108	.120	.108	.115	.086

Table 7 - Measured Vertical Deflection Due to a Uniform Load for Model One

Defl. Pt.	Vertical Deflection, w (x,y), inches p=2 psi q=20 lbs	p=4 psi q=30 lbs	p=6 psi q=50 lbs	p=8 psi q=60 lbs	p=10 psi q=80 lbs	p=10 psi q=60 lbs
28	.19	.21	.24	.23	.25	.19
29	.76	.63	.72	.67	.74	.56
30	1.02	.83	.95	.89	.99	.73
31	-	.18	-	.17	.19	.14
32	.58	.46	.52	.48	.52	.39
33	.75	.60	.68	.64	.70	.52
34	.13	.10	.11	.10	.11	.08
35	.38	.29	.33	.30	.33	.24
36	.50	.37	.41	.39	.42	.31
37	.27	.19	.21	.19	.21	.15
38	.12	.08	-	.06	.07	.05
39	.04	.02	.03	.03	.03	.02

Table 8 - Measured Vertical Deflection Due to a Uniform Load for Model Two

Defl. Pt.	Vertical Deflection, w (x,y), inches p=2 psi q=20 lbs	p=4 psi q=30 lbs	p=6 psi q=30 lbs	p=6 psi q=50 lbs	p=8 psi q=60 lbs	p=10 psi q=60 lbs
28	.26	.20	.16	.26	.23	.18
29	.76	.62	.46	.75	.67	.53
30	.96	.79	.58	.96	.85	.68
31	.18	.15	.10	.18	.16	.12
32	.55	.45	.32	.53	.47	.38
33	.73	.60	.43	.71	.64	.50
34	.13	.10	.07	.12	.11	.08
35	.37	.29	.21	.34	.31	.24
36N	.46	.36	.25	.42	.38	.29
38N	.09	.09	.06	.10	.10	.07

Table 9 - Measured Room Temperature Vibration Frequencies and Mode Shapes for Model One

Mode	Press. psi	Freq. cps	Mode Shape Accelerometer Number					
			29	30	31	33	35	36
1	2	11.3	Not recorded					
1	4	15.0	.95	1.0	.22	.92	1.08	.58
1	6	18.0	.82	1.0	.17	.82	.44	.52
1	8	20.4	.79	1.0	.16	.75	.32	.45
1	10	21.4	.77	1.0	.15	.73	.32	.43
2	2	22.3	.63	.68	.53	.41	1.0	.48
2	4	29.4	.62	1.10	.55	.95	1.0	1.76
2	6	35.3	.18	.38	.15	.30	1.0	.60
2	8	39.9	.34	.38	.14	.29	1.0	.69
2	10	44.1	.52	.52	.17	.36	1.0	.92
3	2	27.9	1.0	.42	.39	.21	.78	.49
3	4	35.2	1.0	.30	.19	.14	.41	.56
3	6	41.9	1.0	.23	.18	.14	.76	.53
3	8	47.1	1.0	.19	.16	.12	.59	.45
3	10	53.0	1.0	.17	.18	.11	.39	.39

Table 10 - Measured Room Temperature Vibration Frequencies and Mode Shapes for Model One After 650°F Test

Mode	Press. psi	Freq. cps.	Mode Shape Accelerometer Number 29	30	31	33	35	36
1	2	13.1	.88	1.00	.16	.74	.43	.16
1	4	14.2	.73	1.00	.12	.58	.28	.09
1	6	14.6	.74	1.00	.11	.59	.25	.12
1	8	16.1	.71	1.00	.10	.54	.22	.12
1	10	17.0	.73	1.00	.10	.55	.20	.12
2	2	24.3	.29	.56	.29	.26	1.00	.60
2	4	29.4	.14	.46	.27	.49	1.00	.95
2	6	34.9	.16	.53	.25	.40	1.00	1.02
2	8	39.8	.25	.59	.21	.33	1.00	1.04
2	10	42.3	.16	.58	.24	.45	1.00	1.06
3	2	28.5	1.00	.46	.32	.15	.79	.71
3	4	37.8	1.00	.30	.27	.06	.62	.64
3	6	43.0	1.00	.31	.23	.07	.65	.68
3	8	47.4	1.00	.34	.19	.08	.76	.77
3	10	52.0	1.00	.27	.19	.08	.69	.71

Table 10 (Cont'd)

Mode	Press. psi	Freq. cps.	Mode Shape Accelerometer Number					
			29	30	31	33	35	36
4	2	37.9	1.05	1.00	.93	.66	.52	.50
4	4	50.3	.94	1.00	.87	.42	.52	.44
4	6	59.8	1.02	1.00	.97	.35	.54	.45
4	8	67.3	.86	1.00	.90	.28	.46	.36
4	10	74.3	.89	1.00	.92	.29	.44	.33
5	2	46.3	.45	.77	.49	.23	1.00	.13
5	4	61.9	.26	.61	.34	.13	1.00	.19
5	6	73.1	.23	.77	.35	.08	1.00	.21
5	8	82.1	.19	.75	.29	.12	1.00	.21
5	10	90.1	.11	.52	.17	.15	1.00	.15
6	2	54.4	.24	1.00	.38	.25	.49	.19
6	4	73.2	.32	1.00	.39	.31	.50	.13
6	6	87.1	.50	1.00	.65	.49	.77	.13
6	8	98.2	.52	1.00	.62	.42	.68	.11
6	10	108.3	.62	1.00	.66	.49	.75	.17

Table 11 - Experimental Natural Frequencies and Damping for Inflatable Model Two

Mode	Frequency, cps (Damping Coefficient, g)										
	p = 2 psi			p = 4 psi	p = 6 psi		p = 8 psi	p = 10 psi		
	Rm Temp	500°F	650°F	Rm Temp	Rm Temp	650°F	Rm Temp	Rm Temp	500°F	650°F
1	10.0 (.147)	10.4 (.088)	13.2 (.044)	12.0 (.147)	13.4 (.147)	15.9	14.0 (.110)	15.5 (.147)	14.9 (.088)	16.9 (.044)
2	17.7 (.110)	18.0 (.088)	22.6 (.055)	23.9 (.088)	27.2 (.110)	29.0	30.3 (.088)	34.2 (.055)	32.6 (.028)	35.0 (.028)
3	23.3 (.073)	23.0 (.055)	25.7 (.030)	30.8 (.073)	36.3 (.055)	38.8	41.8 (.073)	46.4 (.055)	44.8 (.024)	47.9 (.028)
4	31.0 (.088)	31.2 (.017)	33.5 (.014)	41.6 (.073)	50.5 (.037)	51.1	57.0 (.026)	62.9 (.024)	63.4 (.008)	64.5 (.009)
5	36.9 (.055)	35.6 (.014)	38.2 (.008)	49.5 (.049)	59.0 (.073)	59.0	66.2 (.037)	72.1 (.022)	71.1 (.014)	72.7 (.011)
6	41.5 (.063)	42.2 (.028)	45.6 (.010)	55.9 (.073)	67.8 (.044)	69.2	77.9	84.1		86.4 (.009)

Table 12 - Measured Room Temperature Vibration Frequencies and Mode Shapes for Model Two

Mode	Press. psi	Freq. cps	Mode Shape Accelerometer Number 28	29	30	31	32	33	34	35	36N	38N
1	2	10.0	.23	.76	1.00	.10	.57	.79	.07	.32	.15	.07
1	4	11.8	.23	.55	1.00	.13	.53	.73	.14	.28	.13	.06
1	6	13.4	.21	.75	1.00	.13	.42	.67	.07	.26	.10	.06
1	8	13.8	.18	.66	1.00	.12	.40	.66	-	-	.09	.04
1	10	15.5	.20	.67	1.00	.13	.42	.65	.06	.23	.13	.07
2	2	18.1	.19	.35	.49	.36	.92	.59	.27	1.00	-	.28
2	4	23.7	.22	.39	.43	.36	.94	.69	.40	1.00	-	.32
2	6	26.9	.21	.36	.26	.27	.68	.57	-	-	1.00	.24
2	8	31.1	.24	.42	.35	.37	1.05	.80	-	1.00	1.41	.37
2	10	33.7	.23	.41	.30	.35	.95	.78	.35	1.00	1.56	.36
3	2	23.3	.58	1.00	.45	.26	.53	.13	.32	.60	-	.24
3	4	30.9	.56	1.00	.32	.19	.38	.12	.19	.59	.53	.24
3	6	36.4	.62	1.00	.25	.17	.36	.29	.24	.60	-	.31
3	8	42.6	.61	1.00	.18	.21	.45	.13	.17	.49	.59	.25
3	10	46.2	.61	1.00	.17	.24	.36	.07	.20	.56	.81	.29
4	2	31.1	.43	.88	.45	.68	1.00	.73	.45	-	.59	.49
4	4	41.7	.07	.57	.42	.62	1.00	.30	.19	.17	.47	.42
4	6	51.1	.46	.83	.25	.85	1.00	1.15	-	-	.79	.61
4	8	57.1	.14	.61	.27	.60	1.00	.25	.17	-	.39	.47
4	10	62.4	.05	.52	.39	.66	1.00	.20	.15	.13	.37	.41

Table 12 (Cont'd)

Mode	Press. Psi	Freq. cps	Mode Shape									
			Accelerometer Number									
			28	29	30	31	32	33	34	35	36N	38N
5	2	37.1	1.15	1.13	.74	.72	.11	.48	.12	.30	.06	1.00
5	4	49.4	.84	.68	.45	.54	.14	.45	.19	.38	.06	1.00
5	6	59.1	.62	.52	.26	.48	.26	.41	.21	.44	.11	1.00
5	8	66.6	.53	.37	.19	.41	.28	.34	.25	.45	.08	1.00
5	10	72.1	.69	.30	.40	.32	.24	.24	.38	.54	.04	1.00
6	2	41.2	.32	.86	1.00	.74	.22	.15	.22	.25	-	.05
6	4	55.7	.37	.70	1.00	.52	.16	.04	-	.17	-	.06
6	6	68.8	.06	.42	1.00	.57	.19	.07	.07	.13	.06	.01
6	8	77.9	.06	.44	1.00	.56	.14	.16	.14	.09	.09	.02
6	10	84.1	.49	.64	1.00	.42	.18	.35	.53	.11	.37	.22

Table 13 - Measured Elevated Temperature Vibration Frequencies and Mode Shapes for Model Two

Mode	Press. psi	Freq. cps	Temp. °F	Mode Shape									
				Accelerometer Number									
				28	29	30	31	32	33	34	35	36N	38N
1	2	10.0	500	-	-	1.00	.11	.59	.72	.11	.32		.10
1	2	10.7	650	-	-	1.00	.27	.45	.88	-	.43	-	.20
1	6	15.9	650	.37	.79	1.00	-	.47	-	.12	.45	.30	.45
1	10	14.9	500	.13	.63	1.00	.11	.15	.59	.06	.16	.18	.07
2	2	17.6	500	.43	-	.46	.36	.93	.73	.34	1.00	.69	.35
2	2	19.7	650	.06	.10	.62	.32	.74	.49	.41	1.00	.10	.36
2	10	32.3	500	.28	.57	.28	.39	.09	.95	.34	1.00	.95	.35
3	2	24.8	650	.61	1.00	.19	.23	.41	.10	.23	.62	.07	.26
3	10	45.0	500	.38	1.00	.12	.15	.05	.07	.21	.55	.60	.30

Table 14 - Experimental Natural Frequencies (cps) for Inflatable Model Three at Room Temperature

Mode	Frequency, cps				
	p = 2 psi	p = 4 psi	p= 6 psi	p = 8 psi	p = 10 psi
1	14.2	16.8	18.1	19.3	20.6
2	24.7	31.2	35.1	38.2	40.6
3	-	38.9	46.1	51.7	56.8
4	38.1	50.7	59.9	66.8	73.8
5	47.6	58.9	69.4	79.2	86.9
6	52.0	72.3	86.9	97.9	-

Table 15 - Experimental Natural Frequencies (cps) for Inflatable Model Three at Elevated Temperatures

Mode	Frequency, cps					
	p = 4 psi			p = 10 psi		
	300°F	500°F	650°F	300°F	500°F	650°F
1	15.0	14.4	15.1	18.5	17.9	18.5
2	28.0	26.6	27.5	37.1	35.8	37.1
3	36.8	36.0	37.6	53.8	51.5	54.1
4	48.0	46.8	48.3	70.7	69.2	70.6
5	56.4	56.2	58.6	83.8	83.2	85.3
6	71.0	71.0	72.6	100.1	-	-

Table 16 - Experimental Natural Frequencies (cps) for Model Three with Weight Added to Shaker

	Frequency, cps											
	Shaker Alone			0.5 lb. wt.			1.0 lb. wt.			1.5 lb. wt.		
Mode \ Press. psi	2	6	10	2	6	10	2	6	10	2	6	10
1	13.4	18.1	20.6	12.9	16.1	18.5	12.6	15.8	18.8	11.8	15.1	20.5
2	24.1	35.1	40.6	22.9	33.3	39.5	22.6	32.3	39.0	23.4	32.6	40.6
3	-	-	56.8	-	-	56.7	-	-	56.8	-	-	56.6
4	37.5	59.9	73.8	36.8	59.0	72.7	37.1	58.6	73.3	37.4	57.3	73.5
5	46.2	69.4	86.9	46.2	69.5	86.8	46.7	70.1	87.2	46.4	69.0	87.0
6	50.5	86.9	-	50.2	86.3	-	50.7	-	-	50.3	-	-

APPENDIX

Vibration Analyses Using Flexibility Influence Coefficients

The vibration analysis using measured influence coefficients is based on standard procedures described in Reference 13. The equation to be solved is usually written as

$$\frac{1}{\omega^2} \left\{ w \right\} = \left[C \right] \left[m \right] \left\{ w \right\}$$

where w is the deflection of the wing, C is a matrix of flexibility influence coefficients, and m is a diagonal matrix of lumped section masses. The solutions for $\frac{1}{\omega^2}$ are called eigenvalues and the w's associated with the eigenvalues are called eigenvectors.

The mass matrices for inflatable model one are presented in Table 17. The influence coefficient matrices calculated from the measured data by the procedures discussed previously are presented in Tables 18 through 33. The frequencies calculated for inflatable model one are presented in Tables 34 through 41. Tables 42 through 53 contain the eigenvectors from calculations using the tangent-curve influence coefficients.

Table 17 - Mass Matrix for Inflatable Model One

Model Location	Mass (lb sec^2/in)	
	A. Shaker Rod Not Included	B. Shaker Rod Included
28	.000508	.000508
29	.000821	.000821
30	.000648	.001316
31	.000513	.000513
32	.000679	.000679
33	.000707	.000707
34	.000484	.000484
35	.000715	.000715
36	.000570	.000570
37	.000544	.000544
38	.000661	.000661
39	.000479	.000479

Table 18 - Measured Flexibility Influence Coefficients, in/lb., p = 2 psi, Room Temperature
(Tangent-Curve)

.03302	.02040	.02080	.00323	.01146	.01271	0	.00466	.00420	.00122	0	0
.01920	.10560	.08667	.00985	.03667	.05333	.00138	.01390	.01968	.00375	0	0
.02400	.09730	.17455	.01030	.03920	.08000	.00170	.01290	.01970	.00312	0	0
.00595	.01111	.00933	.02280	.01333	.00750	.00156	.00424	.00440	.00065	0	0
.01600	.04242	.04640	.01200	.06349	.04100	.00230	.01540	.01650	.00460	.00084	0
.01731	.05714	.08235	.00640	.03600	.08880	.00260	.01740	.02520	.00830	.00160	0
.00125	.00317	.00325	.00142	.00360	.00320	.02067	.01280	.00440	.00235	.00046	0
.00375	.01390	.01200	.00300	.01470	.01800	.01030	.04900	.02520	.01270	.00318	.00021
.00650	.01947	.01650	.00410	.01660	.02610	.00420	.02160	.05231	.01350	.00320	.00116
.00228	.00444	.00375	.00041	.00570	.00660	.00257	.01140	.01350	.03963	.00615	.00100
0	.00067	0	0	.00103	.00158	0	.00413	.00480	.00882	.02069	0
0	0	0	0	0	0	0	.00123	.00127	.00158	.00103	.01060

Table 19 - Measured Flexibility Influence Coefficients, in/lb, p = 4 psi, Room Temperature
(Tangent-Curve)

.01939	.01395	.01205	.00243	.00781	.00976	0	.00190	.00210	.00063	0	0
.01571	.06045	.05077	.00386	.02276	.03361	.00081	.00605	.00894	.00144	0	0
.01316	.05707	.10909	.00571	.02664	.04821	.00224	.00893	.01360	.00185	0	0
.00217	.00789	.00770	.01333	.00714	.00490	.00069	.00280	.00232	.00046	0	0
.00503	.02565	.02615	.00749	.03429	.02370	.00171	.00940	.01136	.00321	.00070	0
.01000	.03773	.04655	.00602	.02405	.05223	.00179	.01235	.01535	.00363	.00113	0
0	.00216	.00212	.00116	.00198	.00257	.01270	.00747	.00353	.00108	0	0
.00271	.00900	.00984	.00272	.00965	.01125	.00714	.02761	.01561	.00563	.00138	0
.00385	.00886	.01477	.00386	.01217	.01857	.00271	.01567	.02619	.00729	.00118	0
0	.00302	.00203	.00092	.00454	.00460	.00302	.00740	.01022	.02305	.00300	.00058
0	0	0	0	.00107	.00095	.00071	.00150	.00273	.00435	.01280	0
0	0	0	0	0	0	0	.00038	.00060	.00116	.00063	.00652

Table 20 - Measured Flexibility Influence Coefficients, in/lb, p = 6 psi, Room Temperature
(Tangent-Curve)

.01387	.00810	.00627	.00130	.00320	.00431	0	.00101	.00167	.00043	0	0
.00880	.04118	.03259	.00328	.01313	.02097	.00072	.00331	.00795	.00125	0	0
.00833	.03684	.06667	.00389	.01576	.03214	.00096	.00510	.00914	.00141	0	0
.00171	.00343	.00317	.00951	.00404	.00307	.00047	.00103	.00190	.00054	0	0
.00433	.01659	.01606	.00475	.02300	.01575	.00156	.00550	.00736	.00200	.00025	0
.00579	.02400	.02962	.00350	.01406	.03488	.00155	.00599	.01125	.00315	.00065	0
0	.00103	.00114	.00041	.00105	.00164	.00764	.00341	.00240	.00088	0	0
.00178	.00514	.00519	.00138	.00636	.00844	.00411	.01933	.01167	.00500	.00071	0
.00175	.00643	.00741	.00141	.00686	.01216	.00189	.01031	.01875	.00532	.00125	0
0	.00071	.00077	.00073	.00200	.00225	.00081	.00440	.00431	.01463	.00147	0
0	0	0	0	.00043	.00060	0	.00081	.00129	.00245	.00875	0
0	0	0	0	0	0	0	0	.00045	.00050	.00038	.00443

Table 21 - Measured Flexibility Influence Coefficients, in/lb, p = 8 psi, Room Temperature
(Tangent-Curve)

.01050	.00668	.00600	.00056	.00288	.00364	0	.00090	.00145	.00018	0	0
.00670	.03400	.02643	.00253	.01145	.01733	.00101	.00367	.00583	.00076	0	0
.00680	.03125	.05357	.00294	.01333	.02485	.00074	.00480	.00771	.00128	0	0
.00117	.00310	.00277	.00727	.00382	.00271	.00035	.00106	.00138	.00046	0	0
.00400	.01400	.01379	.00378	.01861	.01272	.00120	.00457	.00667	.00162	.00028	0
.00450	.01745	.02388	.00263	.01170	.02722	.00115	.00538	.00925	.00260	.00073	0
0	.00087	.00100	.00033	.00109	.00137	.00645	.00344	.00235	.00072	.00039	0
.00110	.00415	.00398	.00135	.00504	.00652	.00285	.01514	.00980	.00407	.00086	0
.00150	.00585	.00670	.00120	.00563	.00995	.00155	.00856	.01600	.00475	.00064	0
0	.00067	.00064	.00023	.00098	.00230	.00070	.00390	.00396	.01125	.00171	0
0	0	0	0	.00023	.00028	0	.00075	.00085	.00266	.00734	0
0	0	0	0	0	0	0	.00030	.00031	.00055	.00022	.00367

Table 22 - Measured Flexibility Influence Coefficients, in/lb, p = 10 psi, Room Temperature
(Tangent-Curve)

.00921	.00607	.00490	.00096	.00218	.00315	0	.00070	.00126	0	0	0
.00659	.02764	.02345	.00286	.00873	.01400	.00058	.00333	.00496	.00055	0	0
.00678	.02519	.04650	.00200	.01000	.02085	.00080	.00400	.00636	.00090	0	0
.00120	.00283	.00260	.00563	.00320	.00252	.00031	.00095	.00139	.00028	0	0
.00376	.01083	.01230	.00381	.01552	.01039	.00090	.00368	.00574	.00143	.00024	0
.00439	.01515	.02273	.00228	.00909	.02292	.00090	.00517	.00818	.00245	.00043	0
0	.00111	.00100	.00025	.00067	.00121	.00595	.00308	.00180	.00045	0	0
.00115	.00357	.00375	.00121	.00367	.00364	.00260	.01249	.00816	.00390	.00095	0
.00165	.00514	.00540	.00095	.00394	.00740	.00110	.00690	.01389	.00400	.00089	0
0	.00069	.00050	0	.00069	.00193	.00055	.00335	.00404	.01099	.00206	0
0	0	0	0	0	0	0	.00065	.00076	.00200	.00536	0
0	0	0	0	0	0	0	0	.00040	.00067	.00022	.00291

Table 23 - Measured Flexibility Influence Coefficients, in/lb, p = 2 psi, 650°F
(Tangent-Curve)

.02727	.01733	.01750	.00210	.01125	.01100	0	.00233	.00348	.00129	0	0
.01786	.08257	.07002	.00620	.03682	.04434	.00177	.00789	.01625	.00208	0	0
.01765	.07500	.13115	.00600	.03750	.06921	.00325	.01222	.02139	.00380	0	0
.00252	.00648	.00698	.02082	.01227	.00620	.00055	.00295	.00366	.00097	0	0
.01089	.03578	.03581	.01110	.06200	.03553	.00385	.01397	.01800	.00566	.00141	0
.01111	.04839	.06590	.00425	.03571	.05242	.00296	.01560	.02744	.00937	.00132	0
.00051	.00194	.00311	.00082	.00461	.00480	.01827	.01069	.00675	.00379	.00044	0
.00200	.01000	.01340	.00291	.01625	.01813	.01091	.04177	.02893	.01143	.00202	.00058
.00470	.01556	.02133	.00320	.01964	.02981	.00423	.02149	.04813	.01593	.00449	.00058
.00130	.00222	.00340	.00085	.00506	.00943	.00295	.01055	.01667	.03600	.00725	.00102
0	0	0	0	.00109	.00170	.00063	.00160	.00397	.00933	.01813	.00032
0	0	0	0	0	.00033	0	.00074	.00150	.00231	.00095	.01110

Table 24 - Measured Flexibility Influence Coefficients, in/lb, p = 6 psi, 650°F
(Tangent-Curve)

.01420	.00900	.00889	.00159	.00488	.00556	0	.00092	.00164	.00042	0	0
.00980	.04100	.03551	.00311	.01512	.02167	.00091	.00368	.00800	.00100	0	0
.00978	.03449	.06667	.00338	.01795	.03150	.00119	.00521	.01042	.00126	0	0
.00189	.00364	.00337	.01019	.00540	.00369	.00043	.00108	.00203	.00071	0	0
.00515	.01536	.01727	.00457	.02431	.01575	.00152	.00500	.00792	.00221	.00046	0
.00613	.02193	.03210	.00333	.01582	.03500	.00165	.00662	.01266	.00400	.00047	0
.00053	.00128	.00103	.00069	.00153	.00203	.00874	.00396	.00258	.00169	.00013	0
.00188	.00514	.00670	.00173	.00685	.00873	.00440	.01935	.01255	.00529	.00123	.00033
.00314	.00830	.00952	.00167	.00798	.01156	.00214	.00995	.02036	.00605	.00135	.00037
.00087	.00140	.00118	.00069	.00265	.00390	.00112	.00460	.00603	.01725	.00321	.00062
0	0	0	0	.00042	.00082	.00018	.00098	.00140	.00325	.00899	.00030
0	0	0	0	0	0	0	.00039	.00055	.00094	.00053	.00495

Table 25 - Measured Flexibility Influence Coefficients, in/lb, p = 10 psi, 650°F
(Tangent-Curve)

.01020	.00679	.00550	.00113	.00358	.00423	0	.00056	.00130	0	0	0
.00644	.02833	.02234	.00201	.01050	.01489	.00057	.00293	.00495	.00052	0	0
.00643	.02424	.04125	.00192	.01211	.02078	.00069	.00330	.00591	.00069	0	0
.00121	.00257	.00250	.00611	.00389	.00216	.00050	.00082	.00123	.00034	0	0
.00395	.01069	.01094	.00346	.01617	.01056	.00092	.00378	.00527	.00169	.00032	0
.00407	.01444	.01964	.00236	.01067	.02256	.00115	.00476	.00773	.00258	.00037	0
.00037	.00065	.00096	.00037	.00136	.00152	.00636	.00253	.00167	.00099	0	0
.00085	.00342	.00362	.00111	.00420	.00521	.00265	.01275	.00795	.00343	.00077	0
.00170	.00467	.00538	.00115	.00601	.00887	.00146	.00710	.01333	.00455	.00086	0
.00043	.00097	.00097	.00041	.00173	.00259	.00076	.00332	.00388	.01023	.00194	.00034
0	0	0	0	.00030	.00065	0	.00062	.00077	.00255	.00645	.00022
0	0	0	0	0	0	0	.00027	.00038	.00055	.00035	.00358

Table 26 - Measured Flexibility Influence Coefficients, in/lb, p = 2 psi, Room Temperature
(Straight-Line)

.03306	.02990	.02400	.00584	.01406	.01775	0	.00607	.00790	.00267	0	0
.02770	.13875	.09920	.01300	.04560	.05920	.00369	.01700	.02490	.00785	0	0
.02910	.10700	.19000	.01260	.05160	.08300	.00240	.01970	.03080	.00624	0	0
.00667	.01130	.01425	.02350	.01490	.00910	.00230	.00596	.00680	.00300	0	0
.01615	.04560	.04875	.01570	.06380	.04190	.00490	.01880	.02490	.00870	.00195	0
.01813	.06460	.09025	.01110	.04680	.08880	.00470	.02380	.03740	.01190	.00210	0
.00166	.00578	.00560	.00240	.00470	.00710	.02040	.01260	.00820	.00625	.00110	0
.00688	.01670	.01975	.00674	.02010	.02270	.01330	.04840	.03520	.01590	.00496	.00144
.00860	.02600	.02825	.00680	.02610	.03540	.00680	.03360	.05980	.02040	.00520	.00200
.00267	.00625	.00558	.00260	.01050	.01350	.00535	.01850	.02320	.04150	.01115	.00267
0	.00142	0	0	.00380	.00445	0	.00538	.00680	.01180	.02490	0
0	0	0	0	0	0	0	.00147	.00264	.00407	.00192	.01120

Table 27 - Measured Flexibility Influence Coefficients, in/lb, p = 4 psi, Room Temperature (Straight-Line)

.01985	.01624	.01531	.00277	.00853	.00977	0	.00245	.00372	.00129	0	0
.01620	.06903	.05698	.00763	.02515	.03882	.00211	.00865	.01296	.00404	0	0
.01589	.06082	.10993	.00725	.02821	.04865	.00240	.01048	.01584	.00375	0	0
.00324	.00869	.00824	.01509	.00931	.00625	.00075	.00338	.00406	.00125	0	0
.00891	.02581	.02763	.00855	.03455	.02395	.00315	.01022	.01276	.00505	.00098	0
.01019	.03856	.05005	.00645	.02463	.05250	.00297	.01262	.01922	.00713	.00148	0
0	.00245	.00269	.00119	.00312	.00305	.01355	.00794	.00449	.00296	0	0
.00301	.00908	.01039	.00343	.01033	.01245	.00722	.02761	.01845	.00875	.00222	0
.00487	.01342	.01570	.00403	.01452	.01908	.00436	.01822	.03218	.01082	.00273	0
0	.00401	.00342	.00127	.00529	.00599	.00311	.00969	.01209	.02311	.00596	.00141
0	0	0	0	.00109	.00150	.00073	.00278	.00341	.00721	.01322	0
0	0	0	0	0	0	0	.00079	.00121	.00268	.00107	.00656

Table 28 - Measured Flexibility Influence Coefficients, in/lb, p = 6 psi, Room Temperature
(Straight-Line)

.01400	.01068	.01012	.00223	.00590	.00759	0	.00179	.00276	.00070	0	0
.01086	.04712	.04045	.00494	.01662	.02420	.00140	.00581	.00877	.00184	0	0
.01124	.04314	.07863	.00546	.01943	.03331	.00180	.00744	.01080	.00178	0	0
.00206	.00535	.00549	.01016	.00580	.00419	.00072	.00213	.00243	.00068	0	0
.00659	.01793	.02014	.00589	.02300	.01698	.00205	.00700	.00909	.00282	.00090	0
.00721	.02600	.03535	.00459	.01666	.03498	.00227	.00887	.01369	.00415	.00090	0
0	.00162	.00183	.00075	.00190	.00216	.01024	.00489	.00288	.00165	0	0
.00258	.00644	.00737	.00252	.00692	.00858	.00466	.01933	.01335	.00565	.00182	0
.00344	.00967	.01140	.00305	.00886	.01329	.00317	.01218	.02295	.00711	.00238	0
0	.00245	.00191	.00090	.00319	.00474	.00178	.00695	.00895	.01561	.00434	.00078
0	0	0	0	.00080	.00115	0	.00169	.00225	.00419	.00980	0
0	0	0	0	0	0	0	.00070	.00092	.00151	.00088	.00467

Table 29 - Measured Flexibility Influence Coefficients, in/lb, p = 8 psi, Room Temperature (Straight-Line)

.01084	.00867	.00798	.00174	.00443	.00502	0	.00144	.00213	.00053	0	0
.00824	.03682	.02996	.00385	.01295	.01855	.00122	.00445	.00667	.00129	0	0
.00856	.03261	.05732	.00410	.01495	.02585	.00135	.00533	.00804	.00134	0	0
.00169	.00382	.00386	.00839	.00441	.00325	.00057	.00157	.00189	.00067	0	0
.00431	.01340	.01379	.00456	.01861	.01272	.00181	.00538	.00695	.00247	.00059	0
.00547	.01996	.02640	.00349	.01304	.02722	.00168	.00659	.01046	.00324	.00073	0
0	.00134	.00143	.00079	.00157	.00199	.00775	.00359	.00261	.00147	0	0
.00160	.00454	.00515	.00215	.00543	.00652	.00395	.01514	.01012	.00468	.00151	0
.00243	.00715	.00801	.00237	.00705	.00995	.00281	.00967	.01708	.00573	.00183	0
0	.00140	.00124	.00059	.00230	.00321	.00142	.00534	.00654	.01295	.00320	.00067
0	0	0	0	.00050	.00071	0	.00143	.00187	.00344	.00786	0
0	0	0	0	0	0	0	.00053	.00084	.00125	.00069	.00367

Table 30 - Measured Flexibility Influence Coefficients, in/lb, p = 10 psi, Room Temperature
(Straight-Line)

.00921	.00689	.00663	.00130	.00359	.00441	0	.00145	.00167	0	0	0
.00659	.02774	.02600	.00294	.01077	.01544	.00085	.00366	.00555	.00122	0	0
.00678	.02639	.05007	.00329	.01258	.02149	.00103	.00440	.00669	.00098	0	0
.00143	.00297	.00323	.00646	.00355	.00266	.00049	.00140	.00175	.00049	0	0
.00376	.01083	.01248	.00388	.01552	.01070	.00140	.00449	.00576	.00223	.00040	0
.00439	.01599	.02281	.00290	.01108	.02301	.00134	.00547	.00844	.00263	.00058	0
0	.00129	.00142	.00060	.00126	.00135	.00666	.00308	.00236	.00120	0	0
.00129	.00409	.00462	.00173	.00434	.00540	.00318	.01249	.00816	.00400	.00108	0
.00191	.00596	.00724	.00175	.00552	.00830	.00203	.00809	.01432	.00497	.00130	0
0	.00107	.00107	0	.00174	.00285	.00111	.00400	.00544	.01119	.00229	0
0	0	0	0	0	0	0	.00115	.00151	.00294	.00636	0
0	0	0	0	0	0	0	0	.00061	.00109	.00054	.00291

Table 31 - Measured Flexibility Influence Coefficients, in/lb, p = 2 psi, 650°F
(Straight-Line)

.02773	.02060	.01821	.00528	.01147	.01261	0	.00484	.00721	.00215	0	0
.02290	.08257	.07002	.01196	.03481	.04434	.00309	.01513	.02331	.00577	0	0
.02162	.07708	.13115	.01186	.03519	.05823	.00410	.01815	.03059	.00720	0	0
.00440	.00896	.00941	.02082	.01210	.00817	.00112	.00509	.00627	.00202	0	0
.01273	.03607	.03581	.01483	.06346	.03095	.00570	.01695	.02384	.00806	.00205	0
.01466	.04730	.06671	.01021	.03457	.06988	.00522	.02147	.03220	.01206	.00312	0
0	.00349	.00553	.00199	.00487	.00524	.01827	.01069	.00751	.00530	.00103	0
.00388	.01387	.01450	.00668	.01676	.01822	.01221	.04177	.03393	.01424	.00445	.00130
.00705	.02048	.02558	.00713	.02128	.02750	.00784	.02952	.05570	.01850	.00536	.00143
.00184	.00629	.00625	.00286	.00833	.01166	.00529	.01617	.02274	.03600	.00945	.00264
0	0	0	0	.00239	.00302	.00110	.00523	.00699	.01128	.01813	0
0	0	0	0	0	0	0	.00170	.00217	.00319	.00167	.01110

Table 32 - Measured Flexibility Influence Coefficients, in/lb, p = 6 psi, 650°F
(Straight-Line)

.01420	.01020	.00975	.00232	.00531	.00663	0	.00177	.00262	.00078	0	0
.01020	.04511	.03679	.00505	.01557	.02295	.00166	.00568	.00822	.00163	0	0
.01074	.03956	.06842	.00556	.01796	.03275	.00186	.00704	.01062	.00203	0	0
.00229	.00482	.00475	.01049	.00632	.00462	.00078	.00246	.00228	.00083	0	0
.00607	.01706	.01840	.00592	.02431	.01665	.00193	.00623	.00847	.00278	.00069	0
.00731	.02496	.03267	.00541	.01637	.03628	.00245	.00818	.01304	.00415	.00090	0
0	.00160	.00170	.00086	.00186	.00234	.00874	.00508	.00298	.00175	.00052	0
.00235	.00651	.00709	.00278	.00685	.00873	.00455	.01935	.01255	.00558	.00191	.00057
.00312	.00830	.01045	.00275	.00842	.01305	.00289	.01218	.02095	.00687	.00206	.00083
.00085	.00228	.00227	.00114	.00338	.00508	.00214	.00743	.00837	.01725	.00437	.00133
0	0	0	0	.00084	.00117	0	.00191	.00250	.00434	.00899	0
0	0	0	0	0	0	0	.00064	.00065	.00131	.00066	.00544

Table 33 - Measured Flexibility Influence Coefficients, in/lb, p = 10 psi, 650°F
(Straight-Line)

.00952	.00756	.00601	.00148	.00386	.00437	0	.00123	.00187	0	0	0
.00644	.02858	.02265	.00323	.01061	.01500	.00098	.00407	.00531	.00131	0	0
.00719	.02635	.04385	.00342	.01211	.02115	.00131	.00468	.00638	.00141	0	0
.00149	.00306	.00296	.00611	.00389	.00319	.00062	.00152	.00178	.00063	0	0
.00395	.01101	.01122	.00361	.01617	.01056	.00150	.00494	.00551	.00212	.00049	0
.00458	.01618	.02055	.00269	.01095	.02350	.00149	.00556	.00852	.00281	.00075	0
0	.00115	.00138	.00067	.00139	.00153	.00737	.00365	.00225	.00127	0	0
.00126	.00431	.00452	.00153	.00498	.00561	.00337	.01330	.00875	.00431	.00110	0
.00219	.00578	.00638	.00201	.00601	.00887	.00228	.00829	.01428	.00515	.00189	0
.00051	.00148	.00106	.00062	.00206	.00326	.00134	.00482	.00533	.01248	.00288	.00056
0	0	0	0	.00061	.00081	0	.00136	.00159	.00316	.00647	0
0	0	0	0	0	0	0	.00050	.00068	.00109	.00060	.00416

Table 34 - Room Temperature Vibration Frequencies Calculated from Tangent-Curve Influence Coefficients for Model One Not Including the Shaker Rod Mass

Mode	Frequency, cps				
	p = 2 psi	p = 4 psi	p = 6 psi	p = 8 psi	p = 10 psi
1	10.6	13.7	17.1	19.0	20.6
2	21.5	28.1	34.1	37.9	41.5
3	27.4	34.4	43.2	48.5	52.9
4	29.4	42.9	49.3	54.9	57.7
5	33.8	46.0	54.8	62.1	67.8
6	35.8	46.9	58.8	66.0	70.4

Table 35 - 650°F Vibration Frequencies Calculated from Tangent-Curve Influence Coefficients for Model One Not Including the Shaker Rod Mass

Mode	Frequency, cps		
	p = 2 psi	p = 6 psi	p = 10 psi
1	11.8	16.9	20.9
2	22.6	33.8	41.1
3	29.0	43.4	54.0
4	35.2	48.3	60.0
5	37.3	53.9	68.1
6	44.2	56.1	70.3

Table 36 - Room Temperature Vibration Frequencies Calculated from Tangent-Curve Influence Coefficients for Model One Including the Shaker Rod Mass

Mode	Frequency, cps				
	p = 2 psi	p = 4 psi	p = 6 psi	p = 8 psi	p = 10 psi
1	8.8	11.3	14.2	15.8	17.1
2	20.1	26.0	32.1	35.8	39.3
3	25.8	31.9	39.5	44.2	48.8
4	29.3	42.8	49.2	54.6	57.7
5	32.9	45.8	54.0	61.0	66.2
6	35.7	46.8	58.8	65.9	70.2

Table 37 - 650°F Vibration Frequencies Calculated from Tangent-Curve Influence Coefficients for Model One Including the Shaker Rod Mass

Mode	Frequency, cps		
	p = 2 psi	p = 6 psi	p = 10 psi
1	9.9	14.1	17.6
2	21.6	32.1	39.1
3	26.9	39.6	48.9
4	34.3	48.2	59.9
5	37.3	53.4	67.3
6	43.9	55.3	69.1

Table 38 - Room Temperature Vibration Frequencies Calculated from Straight-Line Influence Coefficients for Model One Not Including the Shaker Rod Mass

Mode	Frequency, cps				
	p = 2 psi	p = 4 psi	p = 6 psi	p = 8 psi	p = 10 psi
1	9.9	13.2	15.8	18.2	20.0
2	19.8	26.8	32.1	36.2	40.0
3	23.7	34.6	42.1	47.6	54.3
4	30.2	41.8	49.5	55.2	61.0
5	35.3	44.8	55.6	62.7	67.9
6	35.9	47.2	57.7	64.5	70.6

Table 39 - 650°F Vibration Frequencies Calculated from Straight-Line Influence Coefficients for Model One Not Including the Shaker Rod Mass

Mode	Frequency, cps		
	p = 2 psi	p = 6 psi	p = 10 psi
1	11.6	16.4	20.4
2	21.9	32.7	39.4
3	28.8	43.4	54.3
4	35.1	47.5	59.4
5	36.9	54.9	65.2
6	39.5	56.5	68.9

Table 40 – Room Temperature Vibration Frequencies Calculated from Straight-Line Influence Coefficients for Model One Including the Shaker Rod Mass

Mode	Frequency, cps				
	p = 2 psi	p = 4 psi	p = 6 psi	p = 8 psi	p = 10 psi
1	8.3	11.0	13.1	15.2	16.5
2	18.7	25.1	30.2	34.3	37.7
3	21.6	31.4	38.3	43.2	49.7
4	29.7	41.7	49.5	55.1	61.0
5	34.9	44.4	55.4	62.2	67.4
6	35.7	47.1	57.4	64.0	70.2

Table 41 – 650°F Vibration Frequencies Calculated from Straight-Line Influence Coefficients for Model One Including the Shaker Rod Mass

Mode	Frequency, cps		
	p = 2 psi	p = 6 psi	p = 10 psi
1	9.8	13.8	17.2
2	20.5	31.1	37.3
3	27.2	39.1	48.9
4	34.3	47.3	59.3
5	35.4	53.9	64.5
6	39.4	56.3	68.2

Table 42 - Calculated Room Temperature Eigenvectors for the First Vibration Mode of Model One

m = A Without Shaker Rod Mass
m = B With Shaker Rod Mass

Model Station	Eigenvector									
	p = 2 psi		p = 4 psi		p = 6 psi		p = 8 psi		p = 10 psi	
	m = A	m = B	m = A	m = B	m = A	m = B	m = A	m = B	m = A	m = B
28	.172	.151	.180	.151	.152	.128	.163	.143	.166	.142
29	.709	.624	.673	.587	.701	.616	.711	.625	.709	.627
30	1.000	1.000	1.000	1.000	1.000	1.000	1.000	1.000	1.000	1.000
31	.101	.081	.112	.094	.087	.071	.096	.078	.103	.084
32	.439	.367	.405	.335	.417	.344	.431	.360	.428	.360
33	.647	.576	.635	.548	.649	.565	.622	.551	.659	.590
34	.041	.031	.045	.034	.039	.029	.043	.032	.048	.036
35	.173	.127	.189	.146	.192	.142	.186	.138	.172	.132
36	.220	.166	.241	.195	.235	.182	.250	.197	.238	.186
37	.065	.045	.072	.048	.048	.031	.050	.033	.052	.034
38	.013	.007	.012	.006	.009	.005	.007	.004	.004	.002
39	.002	.001	.001	.001	.001	0	.001	.001	.001	.001

Table 43- Calculated Room Temperature Eigenvectors for the Second Vibration Mode of Model One

m = A Without Shaker Rod Mass
m = B With Shaker Rod Mass

Model Station	Eigenvector									
	p = 2 psi		p = 4 psi		p = 6 psi		p = 8 psi		p = 10 psi	
	m = A	m = B	m = A	m = B	m = A	m = B	m = A	m = B	m = A	m = B
28	.025	.135	.010	.215	-.032	.086	-.058	.052	-.055	.094
29	-.065	.403	-.229	.389	-.262	.154	-.269	.189	-.256	.216
30	-.726	-.624	-.757	-.753	-.534	-.531	-.586	-.551	-.612	-.553
31	.144	.226	.095	.189	.100	.159	.105	.173	.124	.205
32	.457	.737	.528	.862	.397	.651	.381	.636	.439	.700
33	.253	.504	.453	.858	.290	.550	.328	.516	.354	.559
34	.273	.261	.300	.289	.213	.206	.269	.258	.269	.270
35	1.000	1.000	1.000	1.000	1.000	1.000	1.000	1.000	1.000	1.000
36	.873	.950	.937	.957	.849	.891	.882	.914	.922	.984
37	.517	.493	.676	.646	.440	.414	.471	.439	.587	.553
38	.205	.187	.209	.185	.127	.117	.138	.122	.134	.116
39	.042	.037	.038	.031	.019	.016	.033	.029	.033	.030

Table 44 - Calculated Room Temperature Eigenvectors for the Third Vibration Mode of Model One

m = A Without Shaker Rod Mass
m = B With Shaker Rod Mass

Model Station	Eigenvector									
	p = 2 psi		p = 4 psi		p = 6 psi		p = 8 psi		p = 10 psi	
	m = A	m = B	m = A	m = B	m = A	m = B	m = A	m = B	m = A	m = B
28	.244	.228	.365	.340	.341	.318	.289	.258	.424	.378
29	1.000	1.000	.875	1.000	.847	1.000	1.000	1.000	1.000	1.000
30	-.678	-.353	-1.000	-.380	-1.000	-.435	-.989	-.425	-.750	-.371
31	.217	.173	.138	.090	.169	.093	.213	.132	.156	.138
32	.327	.350	.392	.177	.589	.349	.609	.404	.337	.331
33	-.656	-.289	.124	.092	-.045	.077	-.465	-.156	-.576	-.230
34	-.010	-.153	-.126	-.230	-.100	-.181	-.011	-.128	.015	-.094
35	-.080	-.504	-.368	-.714	-.351	-.753	-.022	-.390	.059	-.337
36	-.077	-.323	-.414	-.698	-.306	-.588	-.149	-.374	-.106	-.295
37	-.073	-.313	-.249	-.498	-.209	-.390	-.108	-.271	-.146	-.315
38	-.038	-.140	-.100	-.177	-.071	-.120	-.036	-.092	-.032	-.088
39	-.007	-.032	-.024	-.038	-.013	-.020	-.007	-.022	-.011	-.021

Table 45 - Calculated Room Temperature Eigenvectors for the Fourth Vibration Mode of Model One

m = A Without Shaker Rod Mass
m = B With Shaker Rod Mass

Model Station	Eigenvector									
	p = 2 psi		p = 4psi		p = 6 psi		p = 8 psi		p = 10 psi	
	m = A	m = B	m = A	m = B	m = A	m = B	m = A	m = B	m = A	m = B
28	-.082	-.095	-.052	-.072	-.115	-.206	-.170	-.182	-.281	-.299
29	-.816	-.867	-.641	-.644	-.426	-.603	-.509	-.528	-.807	-.847
30	-.052	-.016	-.130	-.047	-.303	-.121	-.229	-.065	-.041	-.012
31	.169	.159	-.106	-.123	.251	.235	.182	.118	.247	.245
32	1.000	.996	.425	.364	1.000	.988	.618	.434	1.000	1.000
33	.936	1.000	1.000	1.000	.733	1.000	1.000	1.000	.937	.983
34	-.263	-.273	-.361	-.351	-.210	-.247	-.247	-.232	-.198	-.205
35	-.680	-.702	-.752	-.732	-.779	-.940	-.695	-.662	-.572	-.594
36	-.240	-.245	.248	.254	-.251	-.261	-.217	-.181	-.104	-.103
37	-.460	-.313	-.435	-.425	-.427	-.515	-.481	-.420	-.389	-.390
38	-.228	-.140	-.112	-.109	-.130	-.151	-.247	-.216	-.181	-.183
39	-.054	-.056	-.041	-.040	-.026	-.029	-.055	-.049	-.031	-.031

Table 46 - Calculated Room Temperature Eigenvectors for the Fifth Vibration Mode of Model One

m = A Without Shaker Rod Mass
m = B With Shaker Rod Mass

Model Station	Eigenvector									
	p = 2 psi		p = 4 psi		p = 6 psi		p = 8 psi		p = 10 psi	
	m = A	m = B	m = A	m = B	m = A	m = B	m = A	m = B	m = A	m = B
28	-.219	-.215	-.126	-.152	-.031	-.071	-.126	-.134	.123	.089
29	.287	.228	.163	.147	.216	.150	.160	.108	.178	.201
30	-.631	-.226	-.292	-.104	-.417	-.131	-.429	-.150	-.350	-.191
31	-.317	-.388	-.502	-.466	-.318	-.316	-.354	-.391	-.153	-.291
32	-.658	-.879	-1.000	-1.000	-1.000	-1.000	-.886	-1.000	-.525	-1.000
33	1.000	1.000	.873	.779	.829	.739	1.000	.986	.644	.966
34	-.371	-.273	-.166	-.095	-.015	-.004	-.216	-.190	-.450	-.408
35	-.563	-.405	-.295	-.180	-.140	-.105	-.505	-.462	-.870	-.938
36	.506	.367	.218	.193	.256	.234	.252	.246	.251	.380
37	-.238	-.165	.577	.406	-.281	-.195	.135	.155	1.000	.937
38	-.071	-.036	.337	.229	-.078	-.044	.061	.069	.401	.335
39	-.022	-.014	.056	.041	-.005	-.001	-.003	0	.116	.109

Table 47 - Calculated Room Temperature Eigenvectors for the Sixth Vibration Mode of Model One

m = A Without Shaker Rod Mass
m = B With Shaker Rod Mass

Model Station	Eigenvector									
	p = 2 psi		p = 4 psi		p = 6 psi		p = 8 psi		p = 10 psi	
	m = A	m = B	m = A	m = B	m = A	m = B	m = A	m = B	m = A	m = B
28	.094	.068	.054	.053	.042	.062	.085	.077	-.013	.007
29	-.061	-.026	-.116	-.097	-.072	-.046	.006	.025	.008	.024
30	.191	.055	.104	.031	.169	.055	.118	.035	.079	.018
31	.112	.097	.061	.028	.148	.136	.126	.109	.047	.036
32	.349	.333	.379	.313	.341	.295	.276	.238	.272	.220
33	-.375	-.301	-.177	-.107	-.310	-.253	-.308	-.247	-.165	-.105
34	-.201	-.273	-.321	-.324	-.137	-.147	-.092	-.110	-.343	-.357
35	-.399	-.510	-.479	-.488	-.346	-.376	-.234	-.271	-.370	-.417
36	-.056	.050	.040	.052	-.083	-.061	-.198	-.177	-.235	-.188
37	1.000	1.000	1.000	1.000	1.000	1.000	.835	.840	1.000	1.000
38	.533	.539	.639	.637	.671	.686	1.000	1.000	.522	.511
39	.056	.055	.093	.093	.080	.083	.076	.076	.104	.106

Table 48 - Calculated 650°F Eigenvectors for the First Vibration Mode of Model One

m = A Without Shaker Rod Mass
m = B With Shaker Rod Mass

Model Station	Eigenvector					
	p = 2 psi		p = 6 psi		p = 10 psi	
	m = A	m = B	m = A	m = B	m = A	m = B
28	.188	.167	.196	.171	.215	.184
29	.735	.659	.747	.663	.773	.686
30	1.000	1.000	1.000	1.000	1.000	1.000
31	.098	.080	.102	.081	.108	.089
32	.488	.403	.432	.362	.447	.376
33	.641	.587	.675	.598	.663	.591
34	.058	.044	.048	.034	.053	.041
35	.228	.175	.218	.168	.203	.155
36	.312	.251	.279	.222	.278	.218
37	.089	.062	.077	.051	.080	.056
38	.015	.009	.013	.007	.013	.008
39	.004	.002	.002	.001	.002	.001

Table 49 - Calculated 650°F Eigenvectors for the Second Vibration Mode of Model One

m = A Without Shaker Rod Mass
m = B With Shaker Rod Mass

Model Station	Eigenvector					
	p = 2 psi		p = 6 psi		p = 10 psi	
	m = A	m = B	m = A	m = B	m = A	m = B
28	-.068	.026	-.093	.027	-.095	.063
29	-.348	-.003	-.376	.020	-.373	.056
30	-.543	-.474	-.476	-.463	-.574	-.535
31	.113	.170	.113	.184	.104	.168
32	.445	.711	.347	.570	.391	.613
33	.172	.323	.341	.529	.356	.521
34	.311	.305	.264	.269	.270	.263
35	1.000	1.000	1.000	1.000	1.000	.987
36	.876	.920	.815	.877	.962	1.000
37	.602	.578	.579	.570	.560	.541
38	.181	.169	.167	.156	.176	.162
39	.049	.045	.045	.041	.046	.041

Table 50 - Calculated 650°F Eigenvectors for the Third Vibration Mode of Model One

m = A Without Shaker Rod Mass
m = B With Shaker Rod Mass

Model Station	Eigenvector					
	p = 2 psi		p = 6 psi		p = 10 psi	
	m = A	m = B	m = A	m = B	m = A	m = B
28	.201	.309	.378	.331	.500	.445
29	.484	1.000	1.000	1.000	.930	1.000
30	-.831	-.547	-.945	-.392	-1.000	-.470
31	.286	.237	.254	.153	.258	.159
32	1.000	.924	.561	.358	.602	.409
33	-.123	-.021	-.356	-.104	-.470	-.163
34	-.080	-.192	-.021	-.118	-.015	-.106
35	-.259	-.587	-.228	-.543	-.015	-.358
36	-.269	-.480	-.083	-.319	-.097	-.294
37	-.305	-.477	-.117	-.308	-.065	-.230
38	-.104	-.156	-.064	-.112	-.053	-.095
39	-.034	-.048	-.015	-.032	-.008	-.025

Table 51 - Calculated 650°F Eigenvectors for the Fourth Vibration Mode of Model One

Model Station	Eigenvector					
	p = 2 psi		p = 6 psi		p = 10 psi	
	m = A	m = B	m = A	m = B	m = A	m = B
28	-.184	-.143	.026	-.018	.128	.061
29	-1.000	-1.000	-.521	-.654	-.516	-.705
30	.654	.269	-.174	-.060	-.250	-.092
31	.282	.381	.385	.376	.377	.359
32	.653	.955	1.000	1.000	1.000	1.000
33	.140	.021	.517	.675	.588	.853
34	-.002	-.001	-.152	-.176	-.134	-.171
35	-.080	-.101	-.519	-.584	-.772	-.946
36	-.119	-.190	-.313	-.350	-.128	-.135
37	-.568	-.545	-.359	-.395	-.427	-.495
38	-.310	-.273	-.139	-.147	-.189	-.207
39	-.068	-.066	-.056	-.061	-.065	-.076

Table 52 - Calculated 650°F Eigenvectors for the Fifth Vibration Mode of Model One

Model Station	Eigenvector					
	p = 2 psi		p = 6 psi		p = 10 psi	
	m = A	m = B	m = A	m = B	m = A	m = B
28	-.009	.010	-.026	-.155	.110	-.012
29	-.311	-.243	.141	.182	.096	.065
30	.131	.039	-.247	-.158	-.227	-.184
31	.096	.088	-.155	-.377	-.164	-.411
32	.289	.275	-.454	-.948	-.228	-.667
33	.155	.128	.563	1.000	.398	1.000
34	-.388	-.388	-.172	-.184	-.306	-.331
35	-1.000	-1.000	-.697	-.728	-.823	-.882
36	.236	.233	-.016	.031	.125	.252
37	.813	.870	1.000	.940	.977	.634
38	.610	.647	.525	.505	1.000	.696
39	.086	.093	.078	.071	.104	.061

Table 53 - Calculated 650°F Eigenvectors for the Sixth Vibration Mode of Model One

Model Station	Eigenvector					
	p = 2 psi		p = 6 psi		p = 10 psi	
	m = A	m = B	m = A	m = B	m = A	m = B
28	-.472	-.457	-.277	-.244	.021	-.114
29	.013	-.034	.253	.119	.067	-.029
30	-.212	-.089	-.516	-.128	-.521	-.096
31	-.067	-.071	-.399	-.327	-.384	-.206
32	-.032	-.041	-.851	-.653	-.618	-.367
33	.317	.360	1.000	.668	1.000	.537
34	-.521	-.522	.046	.095	-.057	.119
35	-.715	-.736	.162	.382	-.104	.343
36	1.000	1.000	.187	.147	.349	.148
37	-.399	-.418	-.845	-1.000	-.754	-1.000
38	-.400	-.408	-.428	-.505	-.712	-.971
39	-.026	-.030	-.084	-.091	-.098	-.119

UNCLASSIFIED
Security Classification

DOCUMENT CONTROL DATA - R&D

(Security classification of title, body of abstract and indexing annotation must be entered when the overall report is classified)

1. ORIGINATING ACTIVITY (Corporate author)
Air Force Flight Dynamics Laboratory (FDDS)
Wright-Patterson Air Force Base, Ohio

2a. REPORT SECURITY CLASSIFICATION
UNCLASSIFIED

2b. GROUP

3. REPORT TITLE
Stiffness and Vibration Characteristics of Inflatable Delta Wing Models at Temperatures up to 650°F

4. DESCRIPTIVE NOTES (Type of report and inclusive dates)
Final, October 1963 - October 1965

5. AUTHOR(S) (Last name, first name, initial)
Pollock, Samuel J.

6. REPORT DATE	7a. TOTAL NO. OF PAGES	7b. NO. OF REFS
June 1966	94	15

8a. CONTRACT OR GRANT NO.

b. PROJECT NO. 1370

c. Task 137003

d.

9a. ORIGINATOR'S REPORT NUMBER(S)
AFFDL-TR-66-14

9b. OTHER REPORT NO(S) (Any other numbers that may be assigned this report)

10. AVAILABILITY/LIMITATION NOTICES
This document is subject to special export controls and each transmittal to foreign governments or foreign nationals may be made only with prior approval of Air Force Flight Dynamics Laboratory (FDD).

11. SUPPLEMENTARY NOTES
,

12. SPONSORING MILITARY ACTIVITY
Air Force Flight Dynamics Laboratory, FDDS
Wright-Patterson Air Force Base, Ohio

13. ABSTRACT

Stiffness and vibration data were obtained on inflatable Airmat models for various internal pressures from two to ten psi and temperatures up to 650°F. The semi-span 65 degree delta wing models were woven from stainless steel monofilament wire and coated with high temperature silicone elastomer. Deflection and vibration characteristics were predicted using shear theory. Vibration predictions were also made using measured influence coefficients.

Shear theory was found to be in good agreement with experiment for deflections due to uniform load except near the leading edge where experimental deflections were smaller than predicted due to the stiffening effect of the rounded edges. Correlation of shear theory prediction for vibration frequencies with experiment improved as internal pressure increased to 10 psi. Vibration calculations using measured small deflection influence coefficients were in good agreement with experiment.

Temperature effects on model vibration characteristics were determined. Model frequencies decreased as temperature was increased from 70°F to about 300°F. For temperatures from 300°F to 650°F, vibration frequencies increased. At 650°F the vibration frequency for a model without ceramic frits in the silicone elastomer coating was as much as 32 percent higher than the room temperature frequency. For a model with ceramic frits in the silicone elastomer coating the frequency at 650°F was as much as 10 percent lower than the room temperature frequency. Mode shapes did not change appreciably with temperature. Structural damping coefficients decreased with increasing temperature.

DD FORM 1 JAN 64 1473

UNCLASSIFIED
Security Classification

14. KEY WORDS	LINK A		LINK B		LINK C	
	ROLE	WT	ROLE	WT	ROLE	WT
Thermoelasticity						
Inflatable Structures						
Dynamics						

INSTRUCTIONS

1. ORIGINATING ACTIVITY: Enter the name and address of the contractor, subcontractor, grantee, Department of Defense activity or other organization *(corporate author)* issuing the report.

2*a*. REPORT SECURITY CLASSIFICATION: Enter the overall security classification of the report. Indicate whether "Restricted Data" is included. Marking is to be in accordance with appropriate security regulations.

2*b*. GROUP: Automatic downgrading is specified in DoD Directive 5200.10 and Armed Forces Industrial Manual. Enter the group number. Also, when applicable, show that optional markings have been used for Group 3 and Group 4 as authorized.

3. REPORT TITLE: Enter the complete report title in all capital letters. Titles in all cases should be unclassified. If a meaningful title cannot be selected without classification, show title classification in all capitals in parenthesis immediately following the title.

4. DESCRIPTIVE NOTES: If appropriate, enter the type of report, e.g., interim, progress, summary, annual, or final. Give the inclusive dates when a specific reporting period is covered.

5. AUTHOR(S): Enter the name(s) of author(s) as shown on or in the report. Enter last name, first name, middle initial. If military, show rank and branch of service. The name of the principal author is an absolute minimum requirement.

6. REPORT DATE: Enter the date of the report as day, month, year; or month, year. If more than one date appears on the report, use date of publication.

7*a*. TOTAL NUMBER OF PAGES: The total page count should follow normal pagination procedures, i.e., enter the number of pages containing information.

7*b*. NUMBER OF REFERENCES: Enter the total number of references cited in the report.

8*a*. CONTRACT OR GRANT NUMBER: If appropriate, enter the applicable number of the contract or grant under which the report was written.

8*b*, 8*c*, & 8*d*. PROJECT NUMBER: Enter the appropriate military department identification, such as project number, subproject number, system numbers, task number, etc.

9*a*. ORIGINATOR'S REPORT NUMBER(S): Enter the official report number by which the document will be identified and controlled by the originating activity. This number must be unique to this report.

9*b*. OTHER REPORT NUMBER(S): If the report has been assigned any other report numbers *(either by the originator or by the sponsor)*, also enter this number(s).

10. AVAILABILITY/LIMITATION NOTICES: Enter any limitations on further dissemination of the report, other than those imposed by security classification, using standard statements such as:

(1) "Qualified requesters may obtain copies of this report from DDC."

(2) "Foreign announcement and dissemination of this report by DDC is not authorized."

(3) "U. S. Government agencies may obtain copies of this report directly from DDC. Other qualified DDC users shall request through
_______________________________."

(4) "U. S. military agencies may obtain copies of this report directly from DDC. Other qualified users shall request through
_______________________________."

(5) "All distribution of this report is controlled. Qualified DDC users shall request through
_______________________________."

If the report has been furnished to the Office of Technical Services, Department of Commerce, for sale to the public, indicate this fact and enter the price, if known.

11. SUPPLEMENTARY NOTES: Use for additional explanatory notes.

12. SPONSORING MILITARY ACTIVITY: Enter the name of the departmental project office or laboratory sponsoring *(paying for)* the research and development. Include address.

13. ABSTRACT: Enter an abstract giving a brief and factual summary of the document indicative of the report, even though it may also appear elsewhere in the body of the technical report. If additional space is required, a continuation sheet shall be attached.

It is highly desirable that the abstract of classified reports be unclassified. Each paragraph of the abstract shall end with an indication of the military security classification of the information in the paragraph, represented as *(TS)*, *(S)*, *(C)*, or *(U)*.

There is no limitation on the length of the abstract. However, the suggested length is from 150 to 225 words.

14. KEY WORDS: Key words are technically meaningful terms or short phrases that characterize a report and may be used as index entries for cataloging the report. Key words must be selected so that no security classification is required. Identifiers, such as equipment model designation, trade name, military project code name, geographic location, may be used as key words but will be followed by an indication of technical context. The assignment of links, rules, and weights is optional.